nature genetics

Article

https://doi.org/10.1038/s41588-023-01571-z

Pangenome analysis reveals genomic variations associated with domestication traits in broomcorn millet

Received: 30 July 2022

Accepted: 17 October 2023

Published online: 30 November 2023

Check for updates

Jinfeng Chen[1,2,15] ✉, Yang Liu[2,15], Minxuan Liu[1,15], Wenlei Guo[2,3,15], Yongqiang Wang[4,15], Qiang He[1,15], Weiyao Chen[2,3], Yi Liao[5], Wei Zhang[1], Yuanzhu Gao[1], Kongjun Dong[6], Ruiyu Ren[6], Tianyu Yang[6], Liyuan Zhang[7], Mingyu Qi[7], Zhiguang Li[7], Min Zhao[7], Haigang Wang[8], Junjie Wang[8], Zhijun Qiao[8], Haiquan Li[9], Yanmiao Jiang[9], Guoqing Liu[9], Xiaoqiang Song[10], Yarui Deng[10], Hai Li[10], Feng Yan[11], Yang Dong[11], Qingquan Li[11], Tao Li[12], Wenyao Yang[12], Jianghui Cui[13], Hongru Wang[14], Yongfeng Zhou[14], Xiaoming Zhang[2], Guanqing Jia[1], Ping Lu[1], Hui Zhi[1], Sha Tang[1] ✉ & Xianmin Diao[1] ✉

Broomcorn millet (*Panicum miliaceum* L.) is an orphan crop with the potential to improve cereal production and quality, and ensure food security. Here we present the genetic variations, population structure and diversity of a diverse worldwide collection of 516 broomcorn millet genomes. Population analysis indicated that the domesticated broomcorn millet originated from its wild progenitor in China. We then constructed a graph-based pangenome of broomcorn millet based on long-read de novo genome assemblies of 32 representative accessions. Our analysis revealed that the structural variations were highly associated with transposable elements, which influenced gene expression when located in the coding or regulatory regions. We also identified 139 loci associated with 31 key domestication and agronomic traits, including candidate genes and superior haplotypes, such as *LG1*, for panicle architecture. Thus, the study's findings provide foundational resources for developing genomics-assisted breeding programs in broomcorn millet.

Climate change is a severe threat to global food security. Even though high-yielding, resource-efficient major crops have been developed, orphan crops provide an opportunity for climate-resilient agriculture and increased food supply[1,2]. However, despite exhibiting great nutritional diversity under low-input conditions, orphan crops are grown only locally by small and marginal farmers[3–5]. Therefore, studying these crops may help improve the nutritional diversity and environmental resilience of major crops.

Broomcorn millet (*Panicum miliaceum* L.) is an orphan crop mainly cultivated and consumed in the semiarid regions of Asia and Europe[6,7]. It was domesticated in Northern China around 10,000 years before present (BP)[8,9] and was a staple food before the rise of rice and wheat in the area[8,10]. Broomcorn millet spread to Europe at approximately 3,600–4,000 years BP[11–13]. Broomcorn millet has potential as an alternative to major cereals, mainly due to its gluten-free nature, high protein content, and fast-growing and drought-tolerance characteristics[14,15]. However, despite the increasing demand and harvested areas in the United States[16], only a few cultivars have been released to farmers[15,17]. Besides, the genomic diversity of broomcorn millet has not been extensively characterized[18–21] and the genetic basis of its domestication remains to be explored.

Therefore, the present study aimed to analyze the genomes of a worldwide collection of broomcorn millet to identify its origin and

A full list of affiliations appears at the end of the paper. ✉e-mail: chenjinfeng@ioz.ac.cn; tangsha@caas.cn; diaoxianmin@caas.cn

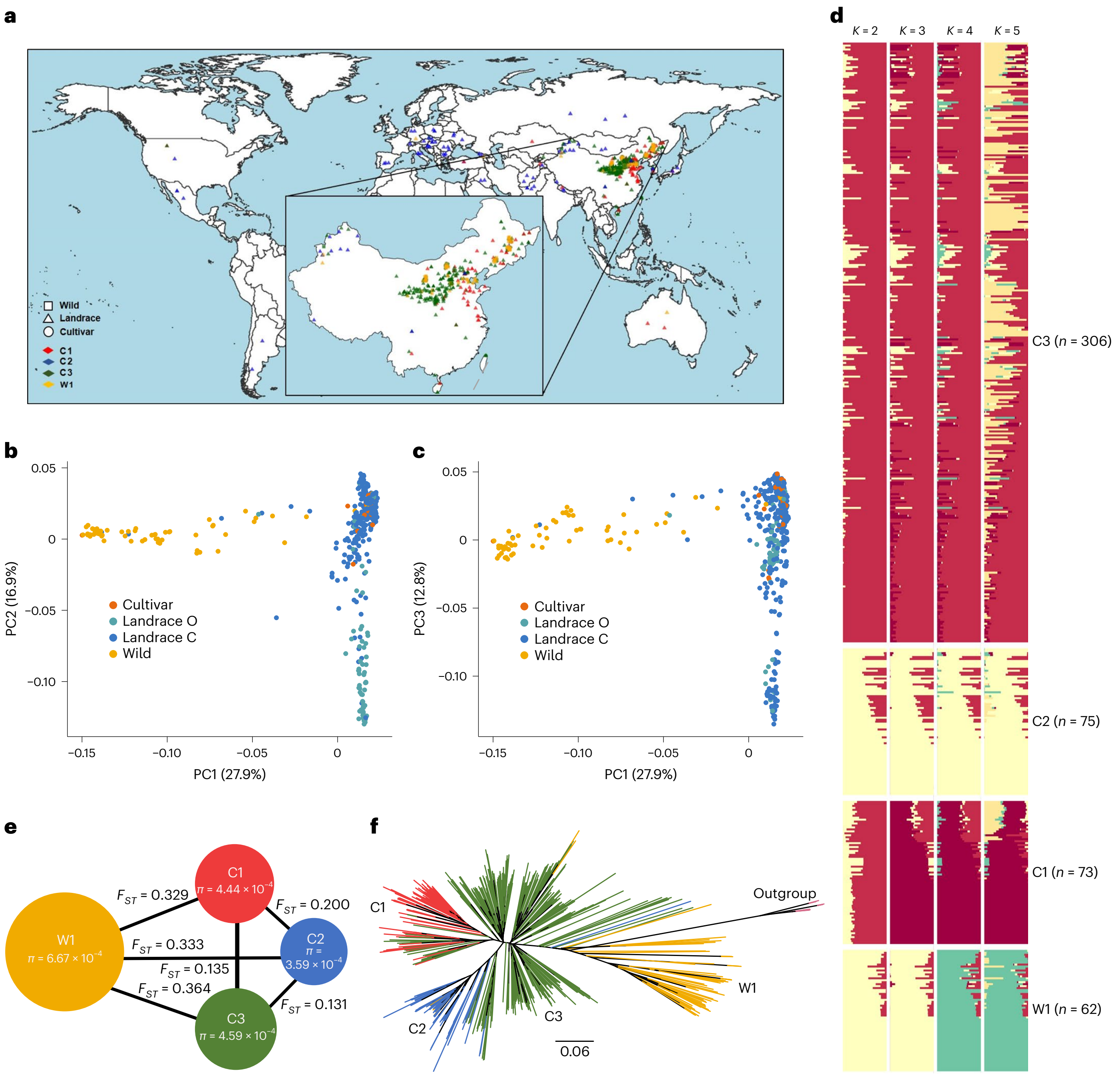

Fig. 1 | Geographical distribution and genomic diversity in broomcorn millet accessions in this study. a, Sample distribution of wild and cultivated broomcorn millet accessions. The squares represent the wild samples, the triangles represent the landraces and the circles represent the cultivars. Different colors represent the population structures inferred based on the resequencing dataset. The geographical map was obtained from Google Maps (https://www.google.com/maps) using the R package ggmap. **b**,**c**, PCA of 516 broomcorn millet accessions. PC1 (27.9%) clearly separates wild accessions from cultivated ones (landraces and cultivars); PC2 (16.9%) (**b**) separates most Chinese landraces (landrace C) from the European and Central Asian landraces (landrace O); and PC3 (12.8%) (**c**) divides the Chinese landraces into two subpopulations. **d**, Ancestral component analysis of broomcorn millet accessions with ADMIXTURE for $K = 2$–5. **e**, π and F_{ST} of broomcorn millet populations. **f**, A maximum likelihood phylogenetic tree of broomcorn millet accessions using switchgrass and foxtail millet (*Setaria italica*) as the outgroups. The colors represent populations identified with ADMIXTURE: 73 C1 (red branches); 75 C2 (blue branches); 306 C3 (green branches); and 62 W1 (brown branches).

explore the genetic basis of agronomic traits related to domestication. We used PacBio high-fidelity (HiFi) reads to generate de novo genome assemblies for 32 representative samples and built a graph-based pangenome to reveal the genomic variations in the broomcorn millet population. We surveyed 43 traits across multiple locations and analyzed the candidate genes associated with domestication and agronomic traits.

Results

Genome sequence, genetic diversity and population structure

To explore broomcorn millet's genetic diversity and population structure, we sequenced the genomes of 516 accessions, including 415 landraces, 38 cultivars and 63 wild accessions using 150-bp paired-end reads (Fig. 1a and Supplementary Table 1). This approach generated 7.6 terabytes of sequencing data (mapping rate = 99.4%; genomic coverage = 97.3%; depth of 17×) (Supplementary Table 2). After mapping these reads to the Longmi4 reference genome[6], we identified 1,890,542 high-quality SNPs and 168,878 insertions and deletions (indels; 1–50 bp). The SNPs were denser in the chromosomal arms than in the pericentromeric regions (Supplementary Fig. 1a), probably due to low selection-associated nucleotide diversity (π) in the low-recombination regions[22,23]. Additionally, the linkage disequilibrium (LD) among SNPs rapidly decreased at 100–200 kb (Supplementary Fig. 2).

To determine population structure, we used principal component analysis (PCA) on 12,816 fourfold degenerate (4DTv) sites and identified the first three principal components (PCs), which accounted for 57.6% of the data variance (Fig. 1b,c). We then used ADMIXTURE[24], STRUCTURE[25], fastSTRUCTURE[26] and discriminant analysis of PC (DAPC)[27] to perform ancestral component analyses on 57,930 pruned high-quality SNPs, optimizing for the number of population clusters. The results demonstrated that the investigated samples could be divided into four clusters: one wild cluster W1; and three cultivated clusters, that is, C1, C2 and C3 (Fig. 1d and Supplementary Figs. 3–5). The largest cluster, C3, contained cultivated accessions from Northwest China, the primary area for broomcorn millet farming. The C1 cluster consisted of cultivated accessions from Northeast and East China, and the C2 cluster included cultivated accessions from European and Central Asian countries (Fig. 1a). These findings indicate that the population structure of broomcorn millet is largely correlated with geographical location.

Further analysis revealed that the π of the cultivated and wild accessions of broomcorn millet (π = 0.00042 and π = 0.00067, respectively; Fig. 1e) were lower than those of rice (π = 0.0024 and π = 0.0030, respectively) and soybean (π = 0.0012 and π = 0.0029, respectively)[28,29]. The cultivated accessions retained 62.6% of the π in their wild relatives. In the phylogenetic tree, the wild population formed a cluster distinct from the three cultivated populations (Fig. 1f). The C3 cluster exhibited higher complexity and was closely related to the wild population, suggesting that the C3 cluster represents the gene pool domesticated from wild accessions. Additionally, a few accessions from Xinjiang and Gansu within the C3 cluster formed the basal lineage or were within the C2 branches (Fig. 1f), suggesting that the European and Central Asian accessions may have originated from Northwest Chinese accessions[30]. We also identified gene flow between cultivated and wild populations (Supplementary Fig. 6). In conclusion, these results suggest that broomcorn millet was domesticated in Northern China and its cultivation subsequently spread to the West from Northwest China.

Pangenome analysis of broomcorn millet

We selected 32 accessions, including 24 cultivated and eight wild ones, representing all major lineages to construct the broomcorn millet pangenome (Fig. 2a). PacBio HiFi reads (35×) were assembled with hifiasm[31] (Supplementary Table 3) and resulted in contigs with N50 ranging from 5.16 to 27.25 Mb (Supplementary Table 3). Finally, we generated 32 chromosome-scale assemblies by anchoring the contigs with Longmi4 (Supplementary Tables 3–5 and Supplementary Fig. 7). Quality assessment revealed 96.0% Benchmarking Universal Single-Copy Orthologs (BUSCO) completeness[32] and a 13.5 long terminal repeat (LTR) assembly index (LAI) score[33] (Supplementary Table 3), suggesting that the genome sequences are of high quality and are highly contiguous.

We further identified an average of 58.1% repetitive sequences per genome (Supplementary Table 6), with larger genomes exhibiting more transposable elements (TEs) (R = 0.92, $P = 8.11 \times 10^{-14}$; Supplementary Fig. 8). Then, using MAKER2 (ref. 34), we annotated an average of 59,332 protein-coding genes per genome, with 95.4% BUSCO completeness (Supplementary Table 7). We identified 27,727 core, 8,288 softcore, 24,494 dispensable and 5,533 private gene families across the 32 genomes (Fig. 2b–d). Core genes showed higher expressions but lower π, and nonsynonymous to synonymous substitution ratios (K_a/K_s), than dispensable and private genes (Fig. 2e–g). Moreover, core genes were enriched with domains related to the basic biological processes, such as RNA recognition motifs ($P = 1.67 \times 10^{-8}$) and helicases ($P = 1.05 \times 10^{-5}$) (Supplementary Table 8). In contrast, dispensable genes were enriched with domains related to enzyme activity and stress resistance, such as leucine-rich repeats ($P \leq 0.05$) (Fig. 2h and Supplementary Table 9). Private genes accounted for 8.4% of gene families in broomcorn millet; however, they contained only 0.4% of protein-coding genes in each accession (Fig. 2c,d). These private gene families may represent lineage-specific genes, and their proportions vary among different species (Supplementary Table 10)[35–37]. Taken together, these results suggest that the dispensable genome of broomcorn millet is enriched with stress resistance genes[35,37] that may contribute substantially to their genomic diversity.

Structural variations in broomcorn millet

To further explore genomic diversity in broomcorn millet, we used an assembly-based method to identify the structural variations (SVs) (>50 bp) in the genomes. We identified 207,033 SVs (Supplementary Table 11 and Fig. 3a) with an accuracy of 87.1% (135 of 155) (Supplementary Tables 12 and 13 and Supplementary Figs. 9 and 10). Subsequently, we merged the SVs from all accessions into 50,689 nonredundant SVs and analyzed the 50,515 presence or absence variants (PAVs) (26,195 deletions, 24,320 insertions) in the rest of the study (Fig. 3b,c and Supplementary Fig. 11). We found that 59.4% (29,998 of 50,515) of PAVs were present in only one or two accessions (Supplementary Fig. 12). This is consistent with low-frequency PAVs in rice and soybean[35,37], suggesting that they represent the newly emerged or deleterious mutations subjected to purifying selection[38]. Besides, unlike SNPs, PAVs displayed no decrease in density in the pericentromeric regions (Supplementary Fig. 1b). Finally, we constructed a graph-based pangenome using 50,515 PAVs and Longmi4 with the vg toolkit[39] and genotyped the PAVs across 516 accessions (Supplementary Figs. 13 and 14). This graph-based pangenome provides a foundation for analyzing the effects of PAVs on the phenotypic variations in broomcorn millet.

We classified the PAVs that overlapped 90% with TEs as TE-derived PAVs; the remaining PAVs were classified as non-TE PAVs. TE-derived PAVs constituted the majority (68.3%) of all PAVs (Fig. 3d and Supplementary Fig. 15a–c). We further annotated PAVs based on their location relative to the protein-coding genes and found that 32.9%

Fig. 2 | Pangenome analysis of 32 broomcorn millet accessions. a, Phylogeny of 516 accessions. The phylogenetic tree was built with SNP data using IQ-TREE. The 32 accessions selected for pangenome analysis are indicated by colored circles in the phylogenetic tree. **b**, Number of pan, core and dispensable gene families. Each number was randomly sampled 100 times. **c**, Composition of the pangenome. The histogram shows the frequency of gene families and the pie chart depicts the proportions of core, softcore, dispensable and private gene families. **d**, Compositions of the individual genomes. Each row represents an accession. **e**, Expressions of core, softcore, dispensable and private genes across 32 accessions. The numbers of core, softcore, dispensable and private genes in the box plot are 1,061,505, 158,766, 417,550 and 6,249, respectively. **f**, Comparison of K_a/K_s values of core, softcore, dispensable and private genes. The numbers of gene pairs in the core, softcore, dispensable and private categories in the box plot are 26,024, 7,214, 15,889 and 2,446, respectively. **g**, Comparison of π of core, softcore and dispensable genes. The numbers of gene families in core, softcore and dispensable in the box plot are 27,609, 8,193 and 24,213, respectively. In **e**,**f**,**g**, the edges and centerlines of the boxes represent the interquartile range (IQR) and medians, with the whiskers extending to the most extreme points (1.5× IQR). Significance was tested using a Kruskal–Wallis test; multiple comparisons were analyzed using a Nemenyi test. The different lowercase letters above the box plots represent significant differences ($P \leq 0.05$). **h**, Top 20 Pfam domains enriched in dispensable genes. The enrichment test was performed based on a hypergeometric distribution. P values were false discovery rate (FDR)-adjusted.

overlapped with the genic regions (Fig. 3e and Supplementary Table 11). Of all non-TE PAVs, 51.7% were located in the genic regions (8,157 genes), while only 13.2% of the TE-derived PAVs were associated with the genic regions (4,458 genes). In addition, the DNA-TE PAVs were closer to the genic regions than the LTR-TE PAVs (10.5 kb versus 35.3 kb; Fig. 3f). To understand how PAVs affect gene function, we compared the expression levels of genes with PAV-affected regions (PAV genes) and those without PAV (non-PAV genes) in each accession, explicitly

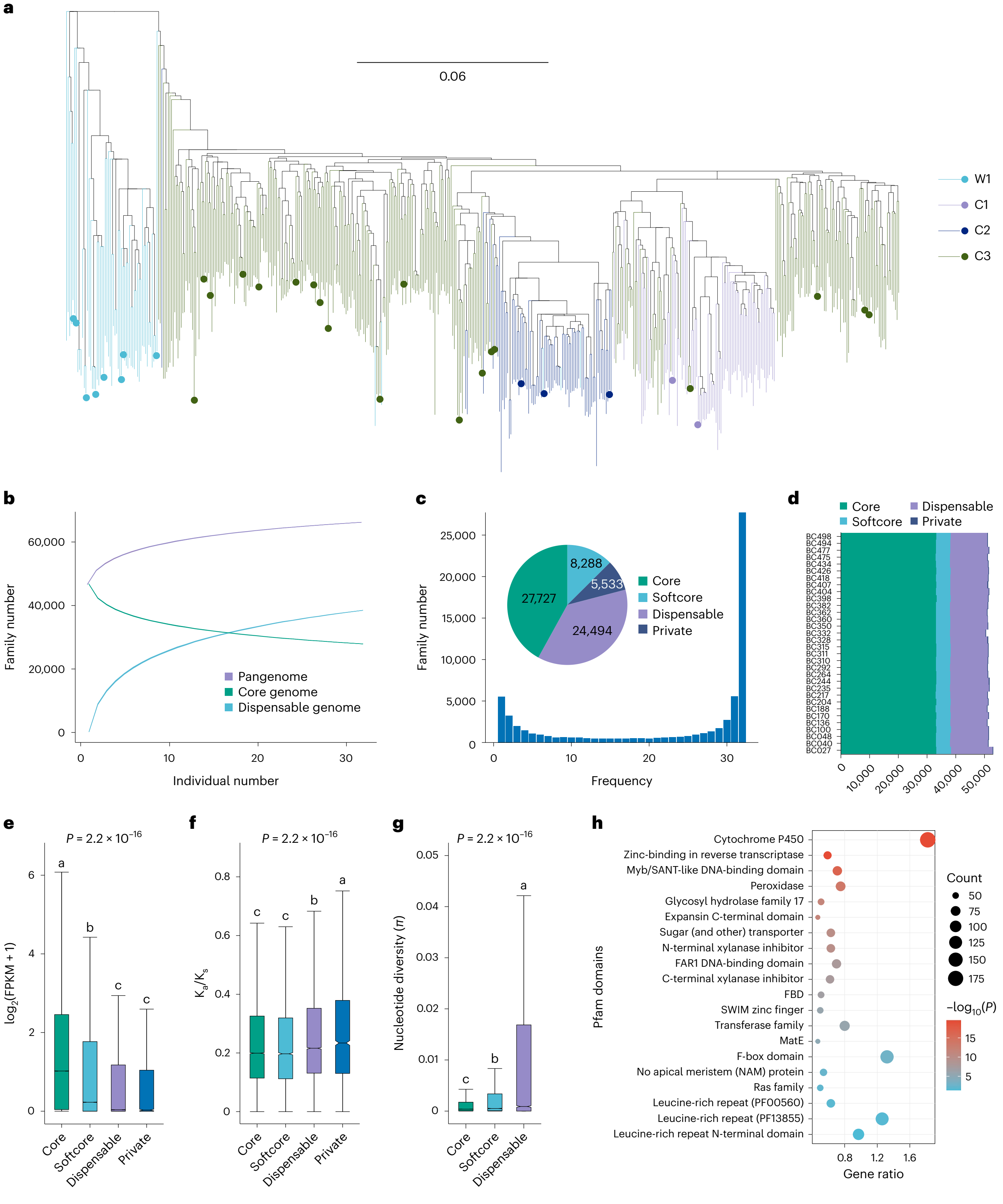

focusing on genes that shared synteny between broomcorn millet and its diploid relative *Panicum hallii*. We found that the expression levels of PAV genes were significantly lower than those of non-PAV genes (5.03 versus 6.42, $P = 2.2 \times 10^{-16}$ in leaves and 4.55 versus 6.45, $P = 2.2 \times 10^{-16}$ in roots) (Supplementary Fig. 16a). Besides, PAV genes had more silenced genes (fragments per kilobase of transcript per million mapped reads (FPKM) < 1) than non-PAV genes ($P = 2.2 \times 10^{-16}$ in leaves; $P = 2.2 \times 10^{-16}$ in roots; Fig. 3g and Supplementary Fig. 16b,c), indicating that PAVs were associated with reduced gene expression in both leaves and roots. Additionally, TE-derived PAVs located in the coding regions and upstream of genes were more likely to affect gene expression than those located in introns and downstream of genes (Fig. 3h, Supplementary Fig. 17 and Supplementary Table 14). Thus, our findings suggest that PAVs influence gene expression by altering the coding and *cis*-regulatory regions.

Furthermore, we identified 648 PAV genes with significantly altered expression levels in the leaves and roots (Supplementary Fig. 18). These differentially expressed PAV genes were enriched with resistance-related domains, such as NB-ARC ($P = 0.002$) and Rx N-terminal domains ($P = 0.007$), which were also PAV gene-enriched Pfam domains (Fig. 3i). We found that resistance genes were located in repeat-rich regions and had a higher frequency of surrounding PAVs than the genome average (Supplementary Fig. 19), suggesting that PAVs are associated with the evolution of resistance genes in broomcorn millet. For instance, in BC027, we found a 4.6-kb insertion between two resistance genes, *longmi055791*, encoding a homologous protein of ENHANCED DISEASE RESISTANCE 2 (ref. 40), and *longmi055792*, encoding an NBS-LRR gene (Fig. 3j). The insertion is associated with decreased expression of both genes (Fig. 3k) and its allele frequency is higher in C2 (73.3%) and C3 (66.0%) populations than in W1 (17.8%) (Fig. 3l). These results suggest that this mutation might have facilitated the adaptation of broomcorn millet to Northwest China (C3) and Europe (C2).

Artificial selection during broomcorn millet domestication

We used a complementary method by integrating a cross-population composite likelihood ratio (XP-CLR)[41], $\pi_{\text{wild}}/\pi_{\text{cultivar}}$ ratio and fixation index (F_{ST}) to detect signals of artificial selection. We compared all cultivated accessions to their wild counterparts and identified 524 genomic regions as targets of artificial selection, covering 30.2 Mb sequences and 3,910 protein-coding genes (Fig. 4a and Supplementary Table 15). These regions overlapped with several known genes linked to domestication and adaptation traits, such as grain yield (*GL3.1*, *SG1* and *GS1*) and flowering time (*Ghd2, Ehd1* and *Hd5*) (Fig. 4a). We found that three cultivated populations (C1, C2 and C3) exhibited distinct selection patterns compared to the wild population (Supplementary Fig. 20). The genes overlapping with the selective regions were enriched in functions related to resistance, such as pathogenesis-related protein 1 and MYC2 in C1, and abscisic acid biosynthesis and calcium-dependent protein kinase in C3 ($P < 0.05$; Supplementary Table 16). These results suggest that each cultivated population developed resistance mechanisms against pathogens, herbivorous insects or drought to adapt to the local environment.

Broomcorn millet is an allopolyploid species containing two subgenomes (A and B)[42]. We found that the selective regions were more abundant and contained more protein-coding genes in subgenome A than in subgenome B (287 versus 237 for selective regions and 2,387 versus 1,523 for selected genes; Supplementary Table 15). We also observed that the protein-coding genes in subgenome B had more PAVs than those in subgenome A (*t*-test, $P = 0.012$ for 2 kb upstream, $P = 0.020$ for 2 kb downstream; $P = 0.009$ for exon and $P = 0.010$ for intron) (Fig. 4b) and showed more differences in expression across tissues (fold change ≥ 1.5; *z*-test $P = 5.95 \times 10^{-3}$ in leaves and $P = 2.56 \times 10^{-3}$ in roots; Supplementary Fig. 21). Furthermore, we analyzed gene loss and pseudogenization events associated with PAVs to understand how PAVs affect gene fractionation in the allopolyploid genome. We identified 1,321 genes deleted or pseudogenized by PAVs (Supplementary Table 17 and Supplementary Fig. 22a,b) and found that subgenome B experienced more gene loss than subgenome A (Supplementary Fig. 22c). This result is consistent with the finding that the TE-rich subgenome B underwent biased gene loss[42], indicating that PAVs facilitated gene fractionation. We also identified 242 gene losses, which were present at a lower frequency in the wild population than in the cultivated population (Supplementary Fig. 22d,e). These results suggest that the ongoing rediploidization in the broomcorn millet genome may have affected gene function, contributing to its domestication.

To better understand how genomic variations affect the function of genes during domestication, we identified 1,099 PAVs in 225 regions under selection, including 39.9% (438 of 1,099) TE-derived PAVs. Among these, 503 PAVs overlapped with the genic regions. We also found 5,663 PAVs with significantly altered allele frequency between wild and cultivated populations during domestication (Supplementary Fig. 15d,e). Integrating PAV-affected genes from the above analyses, we identified 4,930 genes putatively associated with broomcorn millet domestication (Supplementary Table 18). A 6.4-kb TE insertion was identified in the upstream region of *longmi031198* (Fig. 4c), an ortholog of the rice florigen gene *Hd3a*[43]. This mutation (Alt) showed no significant association with the flowering phenotype (Fig. 4d); however, the cultivated population showed an increased allele frequency for the haplotype (Hap) without the insertion (Ref) (Fig. 4c,e). Three closely located deletions (13.4, 3.9 and 13.4 kb) around *longmi040672*, an ortholog of *LAZY1* (ref. 44), were also identified (Fig. 4f). The Hap with the deletion (Alt) was associated with a larger angle between the spike and main stem (Fig. 4g) and was selected against during domestication (Fig. 4h and Supplementary Fig. 23). These results suggest that PAVs, especially

Fig. 3 | SVs in the genomes of 32 broomcorn millet accessions. a, Number of SVs (deletions, insertions, inversions and translocations) in each accession. The proportions of nonredundant SVs are shown in the pie chart. **b**, Histogram showing the length of deletions and insertions (PAVs). **c**, Number of shared and nonredundant PAVs. The accessions are displayed in the following order: BC407, BC404, BC426, BC418, BC382, BC328, BC040, BC027, BC494, BC100, BC498, BC310, BC244, BC311, BC204, BC434, BC292, BC475, BC315, BC477, BC235, BC048, BC136, BC170, BC264, BC362, BC217, BC350, BC188, BC332 and BC360. **d**, Percentage of TE-derived and non-TE PAVs in the broomcorn millet genome. **e**, Percentage of PAVs in the various genomic features. The number of samples in each feature is 32. Each dot represents one accession. **f**, Distance of PAVs to their closest protein-coding genes. The numbers of genes in non-TE PAVs, LTR-TE PAVs and DNA-TEs are 16,001, 30,499 and 1,114, respectively. A two-sided Wilcoxon test was used to determine the significant levels. **g**, Comparison of gene expressions between PAV and non-PAV genes in the leaf tissues of 32 accessions. **h**, Fold change in gene expression between accessions with and without PAVs in the coding region, intron, 2 kb upstream of the start codon and 2 kb downstream of the stop codon of protein-coding genes. The fold change represents the expression change between genes in accessions with or without PAVs. **i**, Pfam enrichment of PAV genes. The enrichment test was performed based on a hypergeometric distribution. *P* values were FDR-adjusted. **j**, A 4.6-kb PAV associated with the disease resistance genes *longmi055791* and *longmi055792*. **k**, Expression of *longmi055791* and *longmi055792* in accessions with (Alt) or without PAV (Ref). A two-sided Wilcoxon test was used to determine the significant levels. The numbers of samples are 16 for Alt and 16 for Ref accessions; each accession consists of three biologically independent plants. **l**, Distribution of the 4.6-kb PAV in the broomcorn millet populations. The number in parentheses represents the number of individuals with unambiguous PAV genotypes in each population. In **e**,**f**,**k**, the edges and centerlines of the boxes represent the IQR and medians, with the whiskers extending to the most extreme points (1.5× IQR).

TE-derived PAVs, may have had an important role in the domestication of broomcorn millet.

Genomic variations associated with domestication

Furthermore, to link genomic and phenotypic variations in broomcorn millet, we measured 43 traits for 516 accessions at seven locations over 2 years (Fig. 5a, Supplementary Fig. 24 and Supplementary Table 19) and conducted genome-wide association studies (GWAS) based on 1,890,542 SNPs and 19,492 PAVs. The SNP-GWAS identified 139 loci significantly associated with 31 traits, including many agronomically important traits, such as seed dimension and plant architecture, as well as those associated

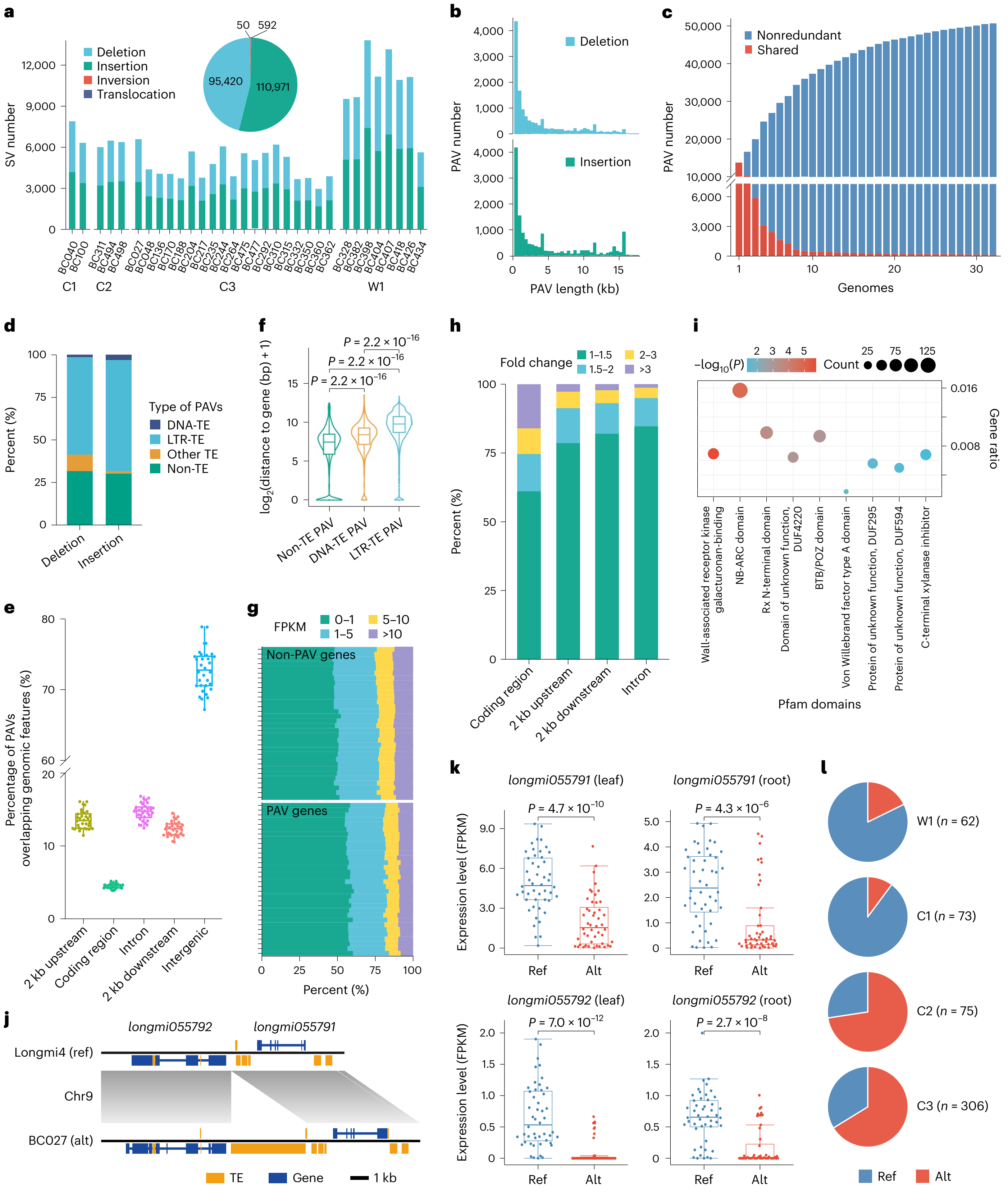

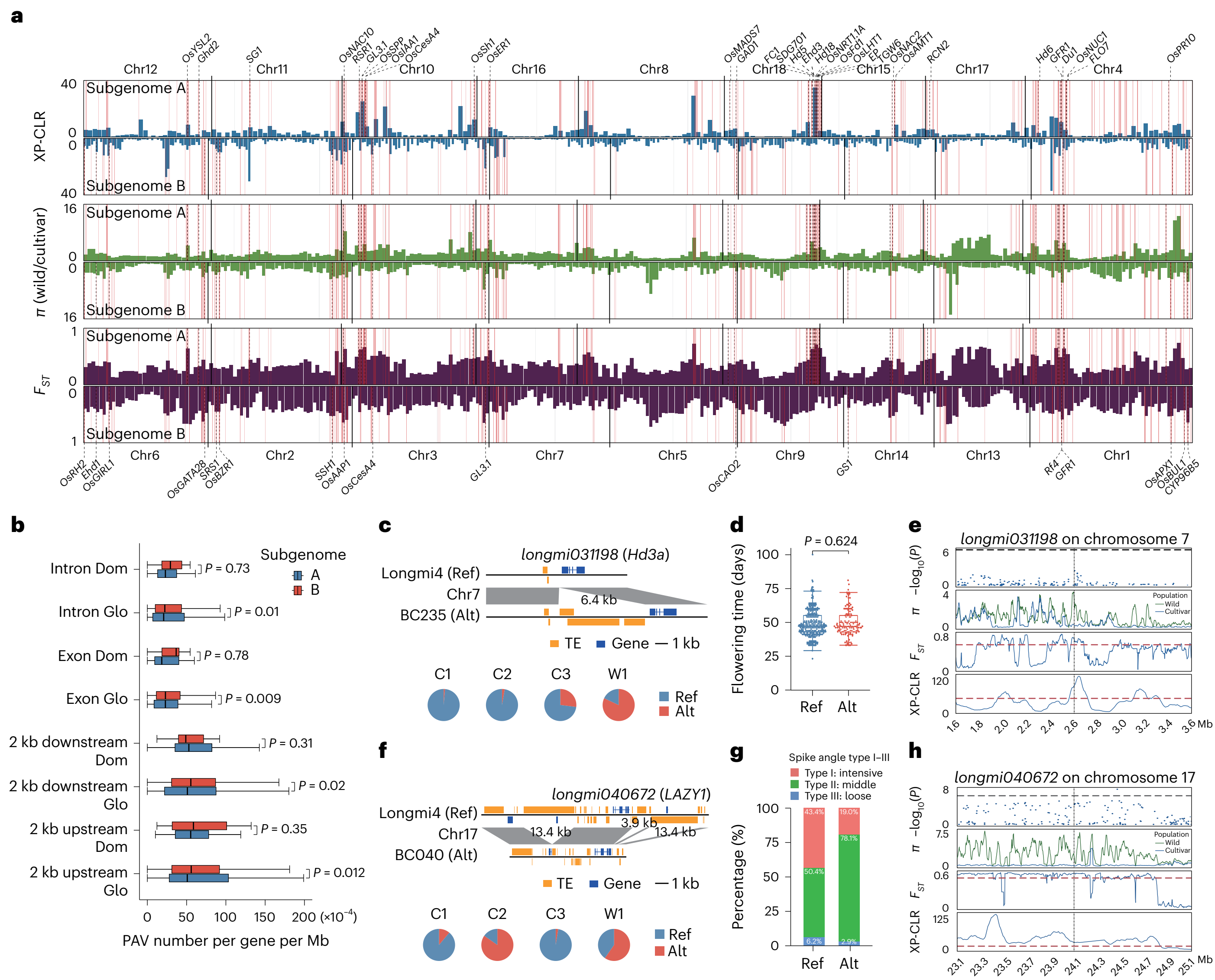

Fig. 4 | Genomic regions under artificial selection during broomcorn millet domestication. **a**, Genome-wide identification of artificial selection regions in domesticated broomcorn millet. From top to bottom, the blue, green and purple peaks represent signals of XP-CLR, *π* and F_{ST}, respectively, in the 20-kb genomic window. Chromosomes of subgenome A were plotted upward in the following order: Chr12, Chr11, Chr10, Chr16, Chr8, Chr18, Chr15, Chr17, Chr4; those of subgenome B were plotted downward in the following order: Chr6, Chr2, Chr3, Chr7, Chr5, Chr9, Chr14, Chr13, Chr1. The red lines represent artificial selection regions identified in this study. Locations of known genes in rice are indicated by their gene symbols. **b**, PAV density in genic features. The densities of PAVs in the artificial selection regions (Dom, *n* = 59) and the whole-genome regions (Glo, *n* = 772) are shown. Significant levels were determined using a two-sided Student's *t*-test. **c**, Comparison of BC235 and Longmi4 sequences with a 6.4-kb insertion at the promoter of *longmi031198* (ortholog of *Hd3a*). The pie charts show the PAV frequencies in the C1, C2, C3 and W1 populations. The allele frequency for the Hap without the insertion is 19.4% in the wild versus 98.6% in C1, 97.3% in C2 and 72.9% in C3. **d**, Flowering time in accessions with the Ref and Alt alleles of *longmi031198*. The number of samples in the Ref and Alt alleles are 375 and 136, respectively. The significance level was determined using a two-sided Wilcoxon test. **e**, GWAS signal, *π*, F_{ST} and XP-CLR in the 1-Mb region of *longmi031198*. The black lines represent the SNP-GWAS significance threshold, which was set at 0.05/total number of SNPs ($P = 2.64 \times 10^{-8}$ or $-\log_{10}(P) = 7.58$). **f**, Comparisons of BC040 and Longmi4 sequences with three closely located deletions (13.4, 3.9 and 13.4 kb) at the *LAZY1* locus. The pie charts show the PAV frequencies in the C1, C2, C3 and W1 populations. **g**, Percentage of angle types (I–III) between the panicle branches and spindle of accessions with Ref and Alt alleles of *longmi040672*. **h**, GWAS signal, *π*, F_{ST} and XP-CLR in the 1-Mb region of *longmi040672*. The black lines represent the SNP-GWAS significance threshold, which was set at 0.05/total number of SNPs ($P = 2.64 \times 10^{-8}$ or $-\log_{10}(P) = 7.58$). In **b**,**d**, the edges and the centerlines of the boxes represent the IQR and medians, with the whiskers extending to the most extreme points (1.5× IQR).

with domestication syndrome, such as seed shattering (SHT) and panicle type (PNT) (Supplementary Table 20). Meanwhile, the PAV-GWAS revealed 70 PAVs associated with 17 traits (Supplementary Table 21). The association signals identified by the PAV-GWAS analysis were consistent with those identified by the SNP-GWAS. The PAV-GWAS only identified a few signals compared to those identified by the SNP-GWAS (Supplementary Fig. 25). However, PAV-GWAS has the potential to identify causal mutations underlying phenotypic variations (Supplementary Fig. 25), making it a complement to the SNP-GWAS in identifying mutations associated with phenotypes[45]. We provide details for the following key traits: seed SHT; inflorescence and seed color; and panicle architecture. They represent domestication syndrome and are crucial for broomcorn millet improvement (Fig. 5b).

Seed SHT. Loss of seed SHT was a crucial step in cereal crop domestication[46]. Phenotypic analysis of the present study indicated that cultivated populations had lower SHT levels than wild accessions (Fig. 5b), suggesting intense selection for the non-SHT phenotype during domestication. To uncover the genetic variations associated with the non-SHT phenotype in cultivated accessions, we examined the homologous genes of 15 known SHT genes of cereal crops (Supplementary Table 22). We found that *longmi009317*, the ortholog of *OsSh1*, which controls seed SHT in rice and sorghum[47], and a related homolog, *longmi003952*, underwent gene loss or pseudogenization in broomcorn millet (Supplementary Fig. 26). A 10.3-kb deletion in *longmi009317* was responsible for the absence of this gene in several C1 and C3 accessions (Supplementary Fig. 26b). Similarly, a 3.2-kb deletion in *longmi003952* led to the loss of six exons (Supplementary Fig. 26f). The frequency of the truncated gene *longmi003952* was higher in C1 (89.0%), C2 (38.7%) and C3 (44.4%) than in W1 (3.2%) (Supplementary Fig. 26f). However, comparing the phenotypes of the accessions carrying the deletion with those carrying wild-type (WT) alleles showed only slight differences in seed SHT (Supplementary Fig. 26h), which implies that the function of the mutated genes was compensated by their homoeologous counterparts (Supplementary Fig. 26i–k). Furthermore, we detected a PAV that truncated *longmi058828*, the ortholog of *OsCAD2* (ref. 48); this mutation was associated with easy SHT (Supplementary Fig. 27a–d). The frequency of the truncated alleles (Ref) in the wild population was greater than in the cultivated populations (Supplementary Fig. 27b). We also identified *longmi012879*, the ortholog of *SSH1*/*OsSNB*[49], in a selective region (Supplementary Fig. 27e). Its Hap 4 was significantly associated with seed SHT in wild accessions (Supplementary Fig. 27f,g). These observations indicate that multiple genomic variations associated with the non-SHT phenotype may have been selected during broomcorn millet domestication.

To identify further genomic variations controlling SHT in broomcorn millet, we analyzed the GWAS data and identified 58 SNPs from 13 chromosomal locations significantly associated with SHT (Supplementary Fig. 28a and Supplementary Table 20). We found two genes, *longmi020192*, encoding pectinesterase (PE) and *longmi028230*, encoding the pectinesterase inhibitor (PEI), in the identified selective sweeps (Fig. 5c and Supplementary Fig. 28b,c,f,g). PE is responsible for pectin degradation in the middle lamella, while PEIs can inhibit the de-esterification of pectin methylesterases. Genes encoding PE have been associated with the abscission of oil palm fruits and bean leaves[50,51], implying similar functions in the abscission zones of broomcorn millet. We identified two nonsynonymous SNPs in the coding regions of *longmi020192* and *longmi028230*. In addition, the Haps carrying these nonsynonymous mutations were highly correlated with seed SHT in wild accessions (Fig. 5d,e and Supplementary Fig. 28d,e,h,i). These findings suggest that *longmi020192* and *longmi028230* have undergone selection for the non-SHT phenotype during broomcorn millet domestication.

Inflorescence and seed color. Inflorescence and seed color are traits associated with plant adaptation, stress response and nutrition content[52,53]. Morphological surveys revealed that green inflorescence and dark-colored seed were preferred in cultivated populations of broomcorn millet (Fig. 5b), indicating the selection of these traits. The SNP-GWAS identified 1,211 SNPs on chromosome 4 associated with inflorescence color (IFC) (Fig. 5f). Two SNPs were found in the regulatory regions of *longmi008332*, encoding a glutathione *S*-transferase (Fig. 5f and Supplementary Fig. 29a), associated with anthocyanin accumulation in plants[54]. These two SNPs formed two major Haps, with most Hap 2 accessions having purple inflorescence and most Hap 1 accessions exhibiting green inflorescence (Supplementary Fig. 29b–f). Moreover, the PAV-GWAS identified a 72-bp insertion in *longmi008332* associated with purple inflorescence (Fig. 5g,h and Supplementary Fig. 25b). All accessions without the insertion (308 of 308) had Hap 1, while 76.6% (128 of 167) of the accessions with this insertion exhibited Hap 2 (Supplementary Fig. 29g), suggesting that the 72-bp insertion was the mutation responsible for purple inflorescence in broomcorn millet.

Several loci associated with seed color (SDC) were detected on chromosomes 5, 6, 9, 11 and 14 in the SNP-GWAS (Supplementary Fig. 30a). Among these, 483 associated SNPs were found on chromosome 9, centered around a tryptophan decarboxylase (*TDC*) gene cluster (*longmi004409*, *longmi004412* and *longmi004413*) (Supplementary Fig. 30a,b). *TDC* is a gene associated with serotonin biosynthesis; its upregulation leads to dark brown seeds or leaves[55]. Hap analysis revealed that Hap 3, 4 and 5, associated with dark seed coats, were present primarily in cultivated accessions (Supplementary Fig. 30c–f). Furthermore, an SNP caused a premature stop codon in *longmi057520* and was highly associated with dark seeds (Supplementary Fig. 31a–e). *Longmi057520* is homologous to *GH2*, synthesizing the coniferyl and sinapyl alcohol precursors in rice[56]. The *GH2* mutant seeds were golden yellow, while the WT seeds were light yellow[56]. Therefore, the premature stop codon in *longmi057520* probably led to dark seed in cultivated broomcorn millet. In addition, *longmi057520* was located in a selective sweep (Supplementary Fig. 31f,g). These observations suggest that SDC is a complex trait controlled by multiple genetic factors that were reformed during broomcorn millet domestication, favoring dark SDCs.

Panicle architecture. Panicle shape is a crucial determinant of grain yield and is a focus of crop domestication and improvement[57,58]. In broomcorn millet, wild accessions have open panicles, while cultivated accessions have closed panicles (Fig. 5b,i), leading to high yields. We conducted the SNP-GWAS analysis on eight panicle shape-related traits (Fig. 5b) and identified 55 genes associated with four panicle-related traits on chromosome 14 (Fig. 5j and Supplementary Fig. 32a,b). Among them, *longmi038370* encodes an SBP-domain protein, an ortholog of *LG1* that controls leaf angle, tassel branch number and tassel branch angle in maize[59], and inflorescence architecture in rice[57,58]. Hap analysis revealed that Hap 1 and 5 were strongly associated with lower inflorescence density (DOI) and larger branches of grain ears and main shafts (Supplementary Fig. 32c–j). Moreover, *longmi038370* was

Fig. 5 | GWAS of genomic variations associated with domestication and agronomically important traits in broomcorn millet. a, Location of seven sites used for phenotype evaluation. The colors represent the yearly rainfall. The geographical map was obtained from ArcGIS (https://www.arcgis.com/index.html). The yearly rainfall data were obtained from WorldClim (https://www.worldclim.org/). **b**, Distribution of SHT, seed and inflorescence (colors), and panicle architecture traits in broomcorn millet. SHT, SDC, IFC, length of panicle stem (LPS), DOI, the branch of the ear of grain and main shaft drift angle (BRM), the branch of ear length (BEL), MED, main panicle length (MPL), projection on branch base (PBB) and PNT are shown. Details of the traits are described in Supplementary Table 19. **c**, Manhattan plot of the GWAS of seed SHT based on the Chifeng 2019 phenotype. **d**,**e**, SHT phenotype of four Haps of *longmi020192* (**d**) and *longmi028230* (**e**). In **d**, the numbers of accessions with the Hap 1, 2, 3 and 4 Haps were 446, 26, 15 and 12, respectively. In **e**, the numbers of accessions with the Hap 1, 2, 3 and 4 Haps were 318, 99, 49 and 37, respectively. **f**, Manhattan plot of GWAS of IFC based on the phenotype collected from Chifeng in 2020. **g**, Comparisons of BC027 and Longmi4 sequences with a 72-bp insertion at the *longmi008332* locus. **h**, Distribution of IFC in Ref and Alt alleles. **i**, Panicles of the representative accessions of wild and cultivated broomcorn millet. **j**, Manhattan plot of the GWAS of MED based on the phenotype collected from Chifeng in 2020. **k**–**o**, Phenotypic analyses of ligule (**k**,**l**) and panicle traits (**m**–**o**) of the *lg-1* mutant and WT plants. The horizontal lines in **c**,**f**,**j** depict the significance threshold ($P = 2.64 \times 10^{-8}$ or $-\log_{10}(P) = 7.58$), which was set at 0.05/*n* (*n* represents the total number of SNPs).

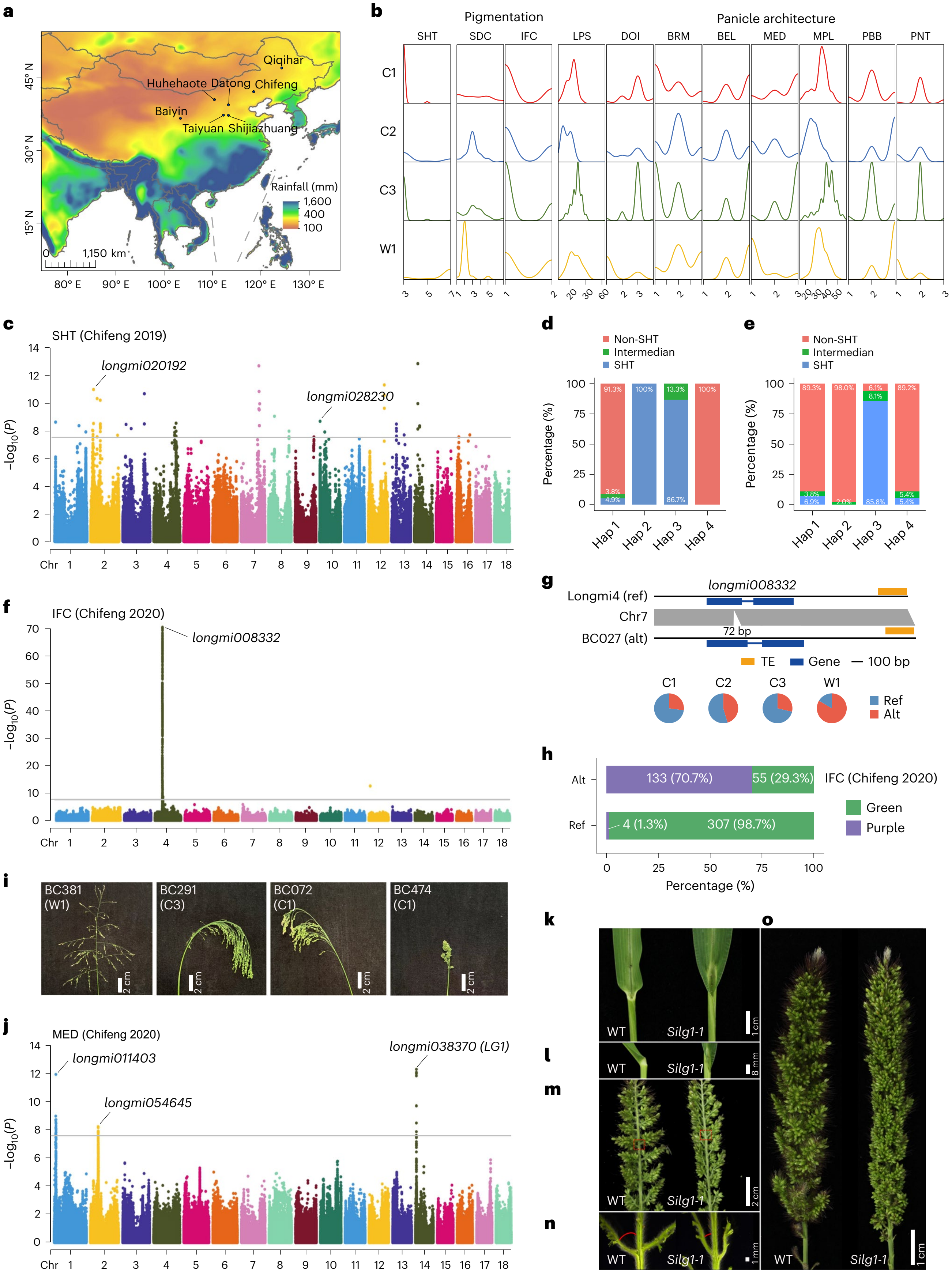
a
Qiqihar
Huhehaote
Datong
Chifeng
Baiyin
Taiyuan
Shijiazhuang
Rainfall (mm)
1,600
400
100
0
1,150 km
45° N
30° N
15° N
80° E
90° E
100° E
110° E
120° E
130° E
b
Pigmentation
Panicle architecture
SHT
SDC
IFC
LPS
DOI
BRM
BEL
MED
MPL
PBB
PNT
C1
C2
C3
W1
c
SHT (Chifeng 2019)
longmi020192
longmi028230
−log10(P)
Chr
d
Non-SHT
Intermedian
SHT
Percentage (%)
91.3%
3.8%
4.9%
100%
13.3%
86.7%
100%
Hap 1
Hap 2
Hap 3
Hap 4
e
Non-SHT
Intermedian
SHT
Percentage (%)
89.3%
3.8%
6.9%
98.0%
2.0%
6.1%
8.1%
85.8%
89.2%
5.4%
5.4%
Hap 1
Hap 2
Hap 3
Hap 4
f
IFC (Chifeng 2020)
longmi008332
−log10(P)
Chr
g
longmi008332
Longmi4 (ref)
Chr7
BC027 (alt)
72 bp
TE
Gene
100 bp
C1
C2
C3
W1
Ref
Alt
h
Alt
Ref
133 (70.7%)
55 (29.3%)
4 (1.3%)
307 (98.7%)
IFC (Chifeng 2020)
Green
Purple
Percentage (%)
i
BC381 (W1)
BC291 (C3)
BC072 (C1)
BC474 (C1)
2 cm
j
MED (Chifeng 2020)
longmi011403
longmi054645
longmi038370 (LG1)
−log10(P)
Chr
k
l
m
n
o
WT
Silg1-1
1 cm
8 mm
2 cm
1 mm

located in a selective sweep (Supplementary Fig. 32k,l), suggesting it was under selection during broomcorn millet domestication. To validate the function of *longmi038370*, we generated three CRISPR–Cas9 mutants of *Seita.3G022100.1* (*SiLG1*), its orthologous gene in foxtail millet (Supplementary Fig. 33a). The *Silg1-1* mutant showed loss of ligule (Fig. 5k,l), a smaller angle between the panicle branch and main stem (Fig. 5m,n and Supplementary Fig. 33b) and compact panicles (Fig. 5o). Thus, we concluded that *longmi038370* controls panicle shape in broomcorn millet.

In addition, we identified loci on chromosomes 1 and 2 associated with the main shaft of ear direction (MED) (Fig. 5j), containing a candidate gene, *longmi054645*, encoding a no apical meristem protein (Supplementary Fig. 34a). Hap analysis revealed that Hap 3 was strongly associated with low MED in wild accessions (Supplementary Fig. 34b–e). Another candidate gene, *longmi011403*, encoding a calcium-dependent phosphotriesterase protein, was also identified on chromosome 1 (Supplementary Fig. 34f). Hap 2 of *longmi011403* was exclusively present in wild accessions; it was associated with lower DOI and open panicles (Supplementary Fig. 34g–l), suggesting that it is pleiotropic and controls multiple panicle traits in broomcorn millet.

Discussion

Broomcorn millet is a promising alternative crop for semiarid regions[6,7,17]. At the start of this study, there were only 14 cultivars in the United States[17] and 222 cultivars in the National Crop Genebank of China, indicating the urgent need for developing a genomics-assisted breeding system in broomcorn millet. We constructed a graph-based pangenome and conducted a GWAS in the population. These data helped us elucidate the domestication history of broomcorn millet and identify genomic signatures underlying domestication and agronomically important traits in broomcorn millet.

Our study clarifies the domestication history of broomcorn millet and directions for future research to resolve its spread routes, which can reveal the origins of agriculture, languages and human societies across the globe[60]. The genomic analyses, corroborated by archaeological evidence from Northern China (8,700–11,500 BP)[9,61], suggest that broomcorn millet was domesticated in Northern China. Xinjiang, a major agricultural and cultural hub between East and West Eurasian countries[62], may have served as an exchange hub for the spread of broomcorn millet. This is supported by evidence of shared variants in ancient DNA from the Xiaohe cemetery (3,400–4,000 BP)[63] and current European accessions. Further studies using additional samples from Gansu, Xinjiang and Eastern Europe may help clarify the spreading routes and their relevant timings. Moreover, researchers found that foxtail millet was domesticated in Northern China slightly later than broomcorn millet, indicating that it may have spread across Eurasia via different routes or at different periods over thousands of years[8,9,64,65]. A study comparing both millets will help reveal when, where and how these crops have spread and adapted across Eurasia. However, these questions cannot be resolved entirely using archaeological remains because of limitations and challenges in processing these datasets[30,64].

Our study also sheds light on the effects of polyploidy on the domestication of broomcorn millet. Recent studies revealed mechanisms on polyploid evolution, such as homoeologous exchanges, selection on coexpression networks and enhanced adaptive abilities driven by gene fractionation[66–68]. Our study revealed that TE-derived PAVs contributed to 68.3% of total PAVs in broomcorn millet. Although most PAVs were deleterious, the polyploid genomes probably buffered these variants by compensating their functions with homoeologous genes. This is evidenced by the observation of deletion or pseudogenization of three homologs of known SHT genes in the wild population of broomcorn millet. Typically, no obvious subgenome dominance in gene expression is detected in the tetraploid broomcorn millet[42]. However, subgenome B contains more TEs and has experienced an excess of gene loss[42]. We found that artificial selection favored subgenome A. Researchers argued that, as in hexaploid wheat, broomcorn millet's subgenome A probably contains more functional genes regulated within subgenome-specific chromatin territories[69]. Thus, the present study's findings with the earlier reports indicate that artificial selection may have driven biased gene expression in one subgenome over the other, leading to unbalanced gene expression between two subgenomes in specific regulatory modules. However, this bias needs to be explored further.

In conclusion, our study has generated a comprehensive dataset that integrates genomic and phenotypic variations in broomcorn millet. The genomic resources described in this study will serve as a foundation for studying the genetic basis of other agronomically important traits, such as nutrient content, salt and drought tolerance, disease and pest resistance in broomcorn millet, and building a genomics-assisted breeding system in broomcorn millet.

Online content

Any methods, additional references, Nature Portfolio reporting summaries, source data, extended data, supplementary information, acknowledgements, peer review information; details of author contributions and competing interests; and statements of data and code availability are available at https://doi.org/10.1038/s41588-023-01571-z.

References

1. Lemmon, Z. H. et al. Rapid improvement of domestication traits in an orphan crop by genome editing. *Nat. Plants* **4**, 766–770 (2018).
2. Ye, C. Y. & Fan, L. Orphan crops and their wild relatives in the genomic era. *Mol. Plant* **14**, 27–39 (2021).
3. Cullis, C. & Kunert, K. J. Unlocking the potential of orphan legumes. *J. Exp. Bot.* **68**, 1895–1903 (2017).
4. Tadele, Z. Orphan crops: their importance and the urgency of improvement. *Planta* **250**, 677–694 (2019).
5. Chiurugwi, T., Kemp, S., Powell, W. & Hickey, L. T. Speed breeding orphan crops. *Theor. Appl. Genet.* **132**, 607–616 (2019).
6. Shi, J. et al. Chromosome conformation capture resolved near complete genome assembly of broomcorn millet. *Nat. Commun.* **10**, 464 (2019).
7. Zou, C. et al. The genome of broomcorn millet. *Nat. Commun.* **10**, 436 (2019).
8. Leipe, C., Long, T., Sergusheva, E. A., Wagner, M. & Tarasov, P. E. Discontinuous spread of millet agriculture in eastern Asia and prehistoric population dynamics. *Sci. Adv.* **5**, eaax6225 (2019).
9. Lu, H. et al. Earliest domestication of common millet (*Panicum miliaceum*) in East Asia extended to 10,000 years ago. *Proc. Natl Acad. Sci. USA* **106**, 7367–7372 (2009).
10. Wang, C.-C. et al. Genomic insights into the formation of human populations in East Asia. *Nature* **591**, 413–419 (2021).
11. Dal Corso, M. et al. Between cereal agriculture and animal husbandry: millet in the early economy of the North Pontic region. *J. World Prehist.* **35**, 321–374 (2022).
12. Filipović, D. et al. New AMS ^{14}C dates track the arrival and spread of broomcorn millet cultivation and agricultural change in prehistoric Europe. *Sci. Rep.* **10**, 13698 (2020).
13. Martin, L. et al. The place of millet in food globalization during Late Prehistory as evidenced by new bioarchaeological data from the Caucasus. *Sci. Rep.* **11**, 13124 (2021).
14. Santra, D. K., Khound, R. & Das, S. *Proso Millet (Panicum miliaceum L.) Breeding: Progress, Challenges and Opportunities* (Springer, 2019).
15. Singh, M. & Sood, S. *Millets and Pseudo Cereals: Genetic Resources and Breeding Advancements* (Woodhead Publishing, 2020).
16. United States Department of Agriculture (USDA) & National Agricultural Statistics Service. *2021 Crop Production* (USDA, 2022).

17. Habiyaremye, C. et al. Proso millet (*Panicum miliaceum* L.) and its potential for cultivation in the Pacific Northwest, U.S.: a review. *Front. Plant Sci.* **7**, 1961 (2017).
18. Xu, Y. et al. Domestication and spread of broomcorn millet (*Panicum miliaceum* L.) revealed by phylogeography of cultivated and weedy populations. *Agronomy* **9**, 835 (2019).
19. Hunt, H. V. et al. Genetic diversity and phylogeography of broomcorn millet (*Panicum miliaceum* L.) across Eurasia. *Mol. Ecol.* **20**, 4756–4771 (2011).
20. Boukail, S. et al. Genome wide association study of agronomic and seed traits in a world collection of proso millet (*Panicum miliaceum* L.). *BMC Plant Biol.* **21**, 330 (2021).
21. Li, C. et al. Genetic divergence and population structure in weedy and cultivated broomcorn millets (*Panicum miliaceum* L.) revealed by specific-locus amplified fragment sequencing (SLAF-Seq). *Front. Plant Sci.* **12**, 688444 (2021).
22. Hellmann, I. et al. Population genetic analysis of shotgun assemblies of genomic sequences from multiple individuals. *Genome Res.* **18**, 1020–1029 (2008).
23. Gore, M. A. et al. A first-generation haplotype map of maize. *Science* **326**, 1115–1117 (2009).
24. Alexander, D. H., Novembre, J. & Lange, K. Fast model-based estimation of ancestry in unrelated individuals. *Genome Res.* **19**, 1655–1664 (2009).
25. Pritchard, J. K., Stephens, M. & Donnelly, P. Inference of population structure using multilocus genotype data. *Genetics* **155**, 945–959 (2000).
26. Raj, A., Stephens, M. & Pritchard, J. K. fastSTRUCTURE: variational inference of population structure in large SNP data sets. *Genetics* **197**, 573–589 (2014).
27. Jombart, T., Devillard, S. & Balloux, F. Discriminant analysis of principal components: a new method for the analysis of genetically structured populations. *BMC Genet.* **11**, 94 (2010).
28. Huang, X. et al. A map of rice genome variation reveals the origin of cultivated rice. *Nature* **490**, 497–501 (2012).
29. Zhou, Z. et al. Resequencing 302 wild and cultivated accessions identifies genes related to domestication and improvement in soybean. *Nat. Biotechnol.* **33**, 408–414 (2015).
30. Stevens, C. J., Shelach-Lavi, G., Zhang, H., Teng, M. & Fuller, D. Q. A model for the domestication of *Panicum miliaceum* (common, proso or broomcorn millet) in China. *Veg. Hist. Archaeobot.* **30**, 21–33 (2021).
31. Cheng, H., Concepcion, G. T., Feng, X., Zhang, H. & Li, H. Haplotype-resolved de novo assembly using phased assembly graphs with hifiasm. *Nat. Methods* **18**, 170–175 (2021).
32. Manni, M., Berkeley, M. R., Seppey, M., Simão, F. A. & Zdobnov, E. M. BUSCO update: novel and streamlined workflows along with broader and deeper phylogenetic coverage for scoring of eukaryotic, prokaryotic, and viral genomes. *Mol. Biol. Evol.* **38**, 4647–4654 (2021).
33. Ou, S., Chen, J. & Jiang, N. Assessing genome assembly quality using the LTR Assembly Index (LAI). *Nucleic Acids Res.* **46**, e126 (2018).
34. Holt, C. & Yandell, M. MAKER2: an annotation pipeline and genome-database management tool for second-generation genome projects. *BMC Bioinformatics* **12**, 491 (2011).
35. Liu, Y. et al. Pan-genome of wild and cultivated soybeans. *Cell* **182**, 162–176 (2020).
36. Hufford, M. B. et al. *De novo* assembly, annotation, and comparative analysis of 26 diverse maize genomes. *Science* **373**, 655–662 (2021).
37. Qin, P. et al. Pan-genome analysis of 33 genetically diverse rice accessions reveals hidden genomic variations. *Cell* **184**, 3542–3558 (2021).
38. Kou, Y. et al. Evolutionary genomics of structural variation in Asian rice (*Oryza sativa*) domestication. *Mol. Biol. Evol.* **37**, 3507–3524 (2020).
39. Garrison, E. et al. Variation graph toolkit improves read mapping by representing genetic variation in the reference. *Nat. Biotechnol.* **36**, 875–879 (2018).
40. Tang, D., Ade, J., Frye, C. A. & Innes, R. W. Regulation of plant defense responses in *Arabidopsis* by EDR2, a PH and START domain-containing protein. *Plant J.* **44**, 245–257 (2005).
41. Chen, H., Patterson, N. & Reich, D. Population differentiation as a test for selective sweeps. *Genome Res.* **20**, 393–402 (2010).
42. Sun, Y. et al. Biased mutations and gene losses underlying diploidization of the tetraploid broomcorn millet genome. *Plant J.* **113**, 787–801 (2023).
43. Tamaki, S., Matsuo, S., Wong, H. L., Yokoi, S. & Shimamoto, K. Hd3a protein is a mobile flowering signal in rice. *Science* **316**, 1033–1036 (2007).
44. Li, P. et al. *LAZY1* controls rice shoot gravitropism through regulating polar auxin transport. *Cell Res.* **17**, 402–410 (2007).
45. Zhou, Y. et al. Graph pangenome captures missing heritability and empowers tomato breeding. *Nature* **606**, 527–534 (2022).
46. Doebley, J. F., Gaut, B. S. & Smith, B. D. The molecular genetics of crop domestication. *Cell* **127**, 1309–1321 (2006).
47. Lin, Z. et al. Parallel domestication of the *Shattering1* genes in cereals. *Nat. Genet.* **44**, 720–724 (2012).
48. Yoon, J., Cho, L.-H., Antt, H. W., Koh, H.-J. & An, G. KNOX protein OSH15 induces grain shattering by repressing lignin biosynthesis genes. *Plant Physiol.* **174**, 312–325 (2017).
49. Jiang, L. et al. The APETALA2-like transcription factor SUPERNUMERARY BRACT controls rice seed shattering and seed size. *Plant Cell* **31**, 17–36 (2019).
50. Niederhuth, C. E., Cho, S. K., Seitz, K. & Walker, J. C. Letting go is never easy: abscission and receptor-like protein kinases. *J. Integr. Plant Biol.* **55**, 1251–1263 (2013).
51. Roongsattham, P. et al. Cellular and pectin dynamics during abscission zone development and ripe fruit abscission of the monocot oil palm. *Front. Plant Sci.* **7**, 540 (2016).
52. Sweeney, M. T. et al. Global dissemination of a single mutation conferring white pericarp in rice. *PLoS Genet.* **3**, e133 (2007).
53. Zhang, D. et al. Elevation of soybean seed oil content through selection for seed coat shininess. *Nat. Plants* **4**, 30–35 (2018).
54. Matsui, K., Tomatsu, T., Kinouchi, S., Suzuki, T. & Sato, T. Identification of a gene encoding glutathione S-transferase that is related to anthocyanin accumulation in buckwheat (*Fagopyrum esculentum*). *J. Plant Physiol.* **231**, 291–296 (2018).
55. Kanjanaphachoat, P. et al. Serotonin accumulation in transgenic rice by over-expressing tryptophan decarboxylase results in a dark brown phenotype and stunted growth. *Plant Mol. Biol.* **78**, 525–543 (2012).
56. Zhang, K. et al. *GOLD HULL AND INTERNODE2* encodes a primarily multifunctional cinnamyl-alcohol dehydrogenase in rice. *Plant Physiol.* **140**, 972–983 (2006).
57. Ishii, T. et al. *OsLG1* regulates a closed panicle trait in domesticated rice. *Nat. Genet.* **45**, 462–465 (2013).
58. Zhu, Z. et al. Genetic control of inflorescence architecture during rice domestication. *Nat. Commun.* **4**, 2200 (2013).
59. Lewis, M. W. et al. Gene regulatory interactions at lateral organ boundaries in maize. *Development* **141**, 4590–4597 (2014).
60. Robbeets, M. et al. Triangulation supports agricultural spread of the Transeurasian languages. *Nature* **599**, 616–621 (2021).
61. Yang, X. et al. Early millet use in northern China. *Proc. Natl Acad. Sci. USA* **109**, 3726–3730 (2012).
62. Zhang, F. et al. The genomic origins of the Bronze Age Tarim Basin mummies. *Nature* **599**, 256–261 (2021).

63. Li, C. et al. Ancient DNA analysis of *Panicum miliaceum* (broomcorn millet) from a Bronze Age cemetery in Xinjiang, China. *Veg. Hist. Archaeobot.* **25**, 469–477 (2016).
64. He, K., Lu, H., Zhang, J. & Wang, C. Holocene spatiotemporal millet agricultural patterns in northern China: a dataset of archaeobotanical macroremains. *Earth Syst. Sci. Data* **14**, 4777–4791 (2022).
65. Hunt, H. V. et al. Millets across Eurasia: chronology and context of early records of the genera *Panicum* and *Setaria* from archaeological sites in the Old World. *Veg. Hist. Archaeobot.* **17**, 5–18 (2008).
66. Lovell, J. T. et al. Genomic mechanisms of climate adaptation in polyploid bioenergy switchgrass. *Nature* **590**, 438–444 (2021).
67. Chen, Z. J. et al. Genomic diversifications of five *Gossypium* allopolyploid species and their impact on cotton improvement. *Nat. Genet.* **52**, 525–533 (2020).
68. Chalhoub, B. et al. Early allopolyploid evolution in the post-Neolithic *Brassica napus* oilseed genome. *Science* **345**, 950–953 (2014).
69. Jia, J. et al. Homology-mediated inter-chromosomal interactions in hexaploid wheat lead to specific subgenome territories following polyploidization and introgression. *Genome Biol.* **22**, 26 (2021).

[1]Institute of Crop Sciences, Chinese Academy of Agricultural Sciences, Beijing, China. [2]State Key Laboratory of Integrated Management of Pest Insects and Rodents, Institute of Zoology, Chinese Academy of Sciences, Beijing, China. [3]University of Chinese Academy of Sciences, Beijing, China. [4]Institute of Cotton, Hebei Academy of Agriculture and Forestry Sciences, Shijiazhuang, China. [5]College of Horticulture, South China Agricultural University, Guangzhou, China. [6]Crop Research Institute, Gansu Academy of Agricultural Sciences, Lanzhou, China. [7]Chifeng Academy of Agricultural and Animal Husbandry Sciences, Chifeng, China. [8]Center for Agricultural Genetic Resources Research, Shanxi Agricultural University, Taiyuan, China. [9]Institute of Millet Crops, Hebei Academy of Agriculture and Forestry Sciences, Shijiazhuang, China. [10]High Latitude Crops Institute to Shanxi Academy, Shanxi Agricultural University (Shanxi Academy of Agricultural Sciences), Datong, China. [11]Qiqihar Sub-academy of Heilongjiang Academy of Agricultural Sciences, Qiqihar, China. [12]Institute of Crop Sciences, Inner Mongolia Academy of Agricultural and Animal Husbandry Sciences, Hohhot, China. [13]College of Agronomy, Hebei Agricultural University, Baoding, China. [14]Shenzhen Branch, Guangdong Laboratory of Lingnan Modern Agriculture, Genome Analysis Laboratory of the Ministry of Agriculture and Rural Affairs, Agricultural Genomics Institute at Shenzhen, Chinese Academy of Agricultural Sciences, Shenzhen, China. [15]These authors contributed equally: Jinfeng Chen, Yang Liu, Minxuan Liu, Wenlei Guo, Yongqiang Wang, Qiang He. ✉e-mail: chenjinfeng@ioz.ac.cn; tangsha@caas.cn; diaoxianmin@caas.cn

Methods

Plant materials, growth conditions and field phenotyping

A total of 516 broomcorn millet accessions were obtained from the National Crop Genebank of China at the Institute of Crop Sciences, Chinese Academy of Agricultural Sciences, Beijing. This diverse collection included 415 landraces, 38 breeding lines and 63 wild accessions, collected from 16 provinces across China and countries such as Afghanistan, Pakistan, Mexico, South Korea, Japan, Russia, France and Belgium, among others. Hence, it covered almost all areas of broomcorn millet cultivation, offering a comprehensive view of the crop's genetic diversity.

To evaluate the phenotype, we planted these accessions at seven sites across China (Fig. 5a), representing diverse environmental conditions, including regions in Heilongjiang (Qiqihar: 47.05° N, 124.33° E), Inner Mongolia (Chifeng: 42.15° N, 118.52° E; Huhehaote: 40.53° N, 110.40° E), Shanxi (Taiyuan: 37.31° N, 112.29° E; Datong: 39.44° N, 113.30° E), Hebei (Shijiazhuang: 37.27° N, 113.30° E) and Gansu (Baiyin: 36.55° N, 104.17° E). Good-quality and plump seeds of uniform size (80 per accession) were sown in the fields in 2019 and 2020. We evaluated 43 phenotypic traits using a quantitative and descriptive method published for descriptors and data standards[70], maintaining three individual plants per accession. Seed dimension traits, such as seed width, length and weight, were analyzed using the SC-G software (Hangzhou Wanshen Detection Technology).

Short-read sequencing, Hi-C sequencing and data processing

Genomic DNA was extracted from the mature leaves of 516 accessions and used to construct 150-bp paired-end sequencing libraries with an insert size of approximately 350 bp, sequenced on an MGISEQ-2000 platform (MGI Tech). Raw reads were filtered with Trimmomatic (v.0.39) to remove low-quality bases and sequencing adapters[71] and the clean reads were aligned to the Longmi4 reference genome using Burrows–Wheeler Aligner (BWA)-MEM in SpeedSeq (v.0.0.2)[72,73] with default parameters. Genomic variations, including SNPs and indels, were identified with the Genome Analysis Toolkit UnifiedGenotyper (v.3.8)[74] and filtered using the following parameters: QD < 2.0; MQ < 40.0; FS > 60.0; AF < 0.05; HaplotypeScore > 13.0; MappingQualityRankSum < −12.5; ReadPosRankSum < −8.0; QUAL < 30.0||DP < 6||DP > 5,000||HRun > 5; MQ0 > = 4 && ((MQ0/(1.0 × DP)) > 0.1) for SNPs and QD < 2.0; ReadPosRankSum < −20.0; FS > 200.0; MQ0 > = 4 && ((MQ0/(1.0 × DP)) > 0.1); QUAL < 30.0||DP < 6||DP > 5,000||HRun > 5 for indels. Finally, clustered SNPs were filtered using the following settings: --clusterSize 3 --clusterWindowSize 10.

The Hi-C libraries were constructed from the seedlings of BC170 and BC418. The seedlings were cut and cross-linked with 2% formaldehyde via vacuum infiltration; glycine was added to the mixture to stop the cross-linking step. Nuclei were purified, digested with 100 units of DpnII and end-labeled via biotinylation with biotin-14-dATP. Ligated DNA was sheared into 300–600-bp fragments, which were end-repaired, A-tailed and purified. Hi-C libraries were quantified and sequenced on a DNBSEQ-T7 platform (MGI Tech). High-quality Hi-C reads were then mapped to the genome with the BWA using the CPU version of Juicer (v.1.6)[75]. After removing multi-mapped and duplicated reads, a Hi-C contact map was generated with Juicer and visualized using the Juicebox Assembly Tools (v.1.11.08)[76]. The Hi-C interaction map was used to evaluate the quality of genome assembly and SVs identified in BC170 and BC418.

Phylogeny and population structure

To determine the phylogenetic relationships among the 516 broomcorn millet accessions, we first obtained 12,816 4DTv sites from the annotated SNP VCF file using ANNOVAR (v.2020-06-08)[77] and then processed them using the script calc_4dTv_in_eff_vcf.py. We then used these 4DTv sites to build a maximum likelihood phylogenetic tree in IQ-TREE (v.2.1.4-beta)[78] using the GTR + R10 model. We also conducted PCA with the 4DTv sites on the 516 broomcorn millet accessions using PLINK (v.1.90b6.18)[79]. We calculated the LD between two SNPs using PopLDDecay (v.3.41)[80] with the following parameters: MaxDist = 500, minor allele frequency (MAF) = 0.01 and Het = 0.8.

Population structure analysis was analyzed using ADMIXTURE (v.1.3.0)[24] with the number of clusters (K) ranging from 2 to 15 based on 57,930 pruned SNPs obtained using PLINK with the parameters --indep-pairwise 50 5 0.2. Then, discriminant analysis of principal components (DAPC)[27] was conducted using adegenet (v.2.1.8)[81] to determine the optimal K in the broomcorn millet population. In the find.clusters() function, we used 300 PCs, which accounted for approximately 90% of the total genetic variability, to identify the cluster number. The Bayesian information criterion curve indicated that 4–9 clusters were reasonable to summarize the data. We also used fastSTRUCTURE (v.1.0)[26] and STRUCTURE (v.2.3.4)[25] to determine the optimal number of clusters. The marginal likelihood of fastSTRUCTURE showed a similar curve with the ADMIXTURE and DAPC analyses, while STRUCTURE identified K = 2 and K = 4 as the optimal number of clusters. We then compared the clusters identified with ADMIXTURE (W1, C1, C2 and C3) with those identified with DAPC, fastSTRUCTURE and STRUCTURE. The results showed that the four clusters identified with ADMIXTURE, DAPC, fastSTRUCTURE and STRUCTURE were consistent, except for a few individuals in the C1 population that were clustered with C3 in the DAPC clusters. Based on these observations, we divided the population into four clusters (W1, C1, C2 and C3) to summarize the population structure of broomcorn millet.

Identification of selective sweeps

The selective sweeps under artificial selection during domestication and improvement were detected by combining the XP-CLR (v.1.0)[41], $\pi_{\text{wild}}/\pi_{\text{cultivar}}$ and the F_{ST}. The XP-CLR analysis was run with the window size, window step and maximum SNPs set to 20 kb, 2 kb, and 300, respectively. The top 5% of the scores was used as a threshold for significance and smoothed using 100-kb windows with 10-kb step sizes for each chromosome. Meanwhile, the π and F_{ST} values were calculated using VCFtools (v.0.1.13)[82] with a 20-kb sliding window and a 2-kb step. We then identified the overlaps among the selective sweeps detected by the XP-CLR, $\pi_{\text{wild}}/\pi_{\text{cultivar}}$ and F_{ST} using BEDTools (v.2.29.1)[83].

Long-read sequencing, assembly and quality assessment

To create the pangenome of broomcorn millet, 32 representative accessions were selected for de novo assembly based on phylogenetic relationship and geographical distribution. Genomic DNA was extracted from the seedlings of these accessions and used to construct PacBio HiFi SMRTbell libraries using the SMRTbell Express Template Prep Kit 2.0 (Pacific Biosciences). The libraries were sequenced on a PacBio Sequel II platform using the circular consensus sequencing mode available through the SMRT Link to generate HiFi long reads. Raw contigs were generated from HiFi long reads using Hifiasm (v.0.14.2-r315)[31] with the following parameters: -l2 -u. Then, to create chromosome-level assemblies, the contigs from each accession were aligned against the Longmi4 genome, and anchored and oriented according to the alignments into the chromosomes using RagTag (v.2.0.1) (https://github.com/malonge/RagTag).

Furthermore, to evaluate assembly quality, we conducted several analyses. First, we assessed the gene completeness with BUSCO (v.4.0.6)[32] using the embryophyta_odb10 database and repeat completeness based on the LAI[33] using LTR_retriever (v.2.9.0)[84]. Then, we measured *k*-mer completeness, base pair quality value and false duplication using Merqury (v.1.3)[85]. We also identified and evaluated large SVs between the assembly and the Longmi4 genome. HiFi long reads were mapped to the breakpoints of these SVs using Minimap2 (v.2.24-r1122)[86] and manually inspected in the Integrative Genomics Viewer (v.2.9.2)[87]. The assemblies were evaluated based on the HiFi read alignments of 32 accessions at 304 loci (3–17 kb) with genomic differences from Longmi4. Finally, the BC170 and BC418 Hi-C reads were aligned to the corresponding genomes to manually inspect for large SVs of BC170 and BC418, using Juicebox (v.1.11.08)[76]. We evaluated the assemblies using Hi-C chromatin maps of these two accessions (BC170 and BC418) at 22 loci (197–6,114 kb) with genomic differences from Longmi4.

Gene and transposable element annotation

The protein-coding genes in each genome were annotated using the MAKER2 pipeline (v.2.31.11)[34], which uses ab initio prediction, transcriptome evidence and homologous protein evidence. Specifically, AUGUSTUS (v.3.4.0)[88] and SNAP (v.2006-07-28)[89] were used for ab initio gene prediction based on a generalized Hidden Markov Model using a high-confidence gene set from full-length transcriptome data (BioProject ID: PRJNA872304). The transcriptome evidence included RNA sequencing (RNA-seq) datasets from the leaf tissues of each accession as well as inflorescence, leaf blade, leaf sheath, root, mature seed, seedling, shoot and stem of the Pm_0390 cultivar (BioProject ID: PRJNA431485). The raw reads were processed with Trimmomatic (v.0.39)[71] to remove adapters and low-quality reads and mapped to the corresponding genome using HISAT2 (v.2.1.0)[90] with the following parameters: --min-intronlen 20 --max-intronlen 15,000. The full-length transcript sequences of each genome were assembled using StringTie2 (v.2.1.7)[91] with default parameters. The homologous protein evidence was obtained from *P. miliaceum* (Longmi4), *P. hallii*, foxtail millet, *Sorghum bicolor*, *Brachypodium distachyon* and *Arabidopsis thaliana*, and the UniProt proteins of Embryophyta. Protein-coding genes were functionally annotated using InterProScan (v.5.52-86.0)[92]. Finally, repetitive sequences in each genome were identified and classified using RepeatModeler (v.2.0.1)[93] and annotated with RepeatMasker (v.4.0.9) (http://www.repeatmasker.org) with the following parameters: -e rmblast -div 40 -norna.

Gene-based pangenome analyses

A gene-based pangenome of 32 broomcorn millet accessions was constructed according to the gene family clustering strategy. First, protein sequences with 100% similarity in each genome were removed using Cd-hit (v.4.8.1)[94] with the following parameters: -c 1 -aS 1. Then, nonredundant protein sequences were clustered into gene families using OrthoFinder (v.2.5.4)[95]. The resulting gene families were classified into core, softcore, dispensable private genes based on their presence in each of the 32 genomes. Gene families in all 32 genomes were defined as core genes, those in 30–31 as softcore genes, those in 2–29 as dispensable genes and those in only one genome as private genes. The ratio of nonsynonymous to synonymous substitution (K_a/K_s) for each gene of the pangenome was calculated with the KaKs_Calculator (v.2.0)[96] using foxtail millet *Setaria italica* as an outgroup based on multiple sequence alignments performed with ParaAT (v2.0)[97]. The π for each gene of the pangenome was calculated using in-house Perl scripts based on multiple sequence alignments performed with MAFFT (v.7.475)[98]. The following formula was used to calculate π: $\pi = D/L/(N \times (N-1)/2)$, where D represents the number of differential sites, L represents the length of the conserved alignment and N represents the number of sequences.

SV identification and quality assessment

We used a reference-based alignment method called PoPASSYSV (https://github.com/yiliao1022/PoPASSYSV) to perform SV calling on 32 genome assemblies. We aligned each query genome against the Longmi4 genome reciprocally using Minimap2 (v.2.17)[86]. We then used the CHAIN/NET/NETSYNTENY tools (https://github.com/ucscGenomeBrowser/kent) to filter out nonorthologous and nonsyntenic alignments, which are not represented in a single coverage for either the reference or the query. The resulting netsyntenic format files obtained from each pairwise comparison were used to call the five subtypes of SVs, including insertion, deletion, inversion, tandem duplication and complex types, using the PairwiseCalling.pl function within the PoPASSYSV toolkit. To filter out any false positives in SV identification, we excluded deletions and insertions that overlapped with the sequencing gaps or centromere repeats, and inversions that overlapped with the gaps within the 10-bp range. Finally, the SVs identified from 32 assemblies were merged to create the consensus SVs for the broomcorn millet population. All deletions and inversions with an overlapping ratio greater than 90% were merged, while insertions with a distance of less than 10 bp and an identity greater than 80% were merged. The merged deletions and insertions (PAVs) were then genotyped across the 516 accessions based on short-read data using Paragraph (v.2.3)[99] and the vg toolkit (v.1.43.0)[39].

SV quality was assessed using two approaches based on HiFi read alignment and Hi-C chromatin maps in BC170 and BC418 (Supplementary Tables 12 and 13). To evaluate the PAVs missing in the primary assemblies, alternate contigs from 32 accessions, with sizes ranging from 13 Mb to 1.3 Gb, were used for PAV calling (Supplementary Table 3). A total of 21,256 nonredundant PAVs were identified from these alternate contigs, including 11,047 deletions and 10,209 insertions; 4,911 PAVs (23.1%) were absent in the primary assembly dataset. The accuracy of these PAVs was further evaluated by manually inspecting the PacBio long reads mapped at the breakpoints. The analysis revealed a lower accuracy rate of 51.7% (31 of 60), which is lower compared to those in the primary assemblies (83.3%) (Supplementary Table 12). Therefore, despite providing 9.7% (4,911 of 50,515) more total PAVs, these alternate PAVs were not included in the final analysis because of the false positive SV calls.

Pangenome graph construction and PAV genotyping

We constructed a graph-based pangenome using 50,515 PAVs and Longmi4 with the vg toolkit and genotyped the PAVs across 516 accessions using short reads. The short reads were first mapped to the pangenome graph using the giraffe function; then, the read support was computed applying the pack function. PAVs were genotyped across each accession using the call function. The precision, recall and F1 score of the PAVs were computed as 0.64, 0.66 and 0.65, respectively. After removing the PAVs containing 90% repeat sequences, the precision, recall and F1 score of all PAVs were computed as 0.69, 0.71 and 0.70, respectively. The genotyping rate of the PAVs was 79.9% (ranging from 69.8% to 85.0%), and the average depth of short reads for the 516 accessions was around 17× (ranging from 9.9× to 28.7×). As 90% of 516 accessions with read coverage ranging from 12.6× to 22.1×, their genotyping rate ranged from 78.6% to 83.2%.

RNA-seq and differential gene expression analysis

Leaf and root tissues were collected from eight wild and 24 cultivated accessions, maintaining three biological independent experiments per accession. Total mRNA was extracted from these samples using TRIzol reagent (Thermo Fisher Scientific); RNA-seq libraries were prepared for paired-end sequencing on an MGISEQ-2000 platform. Raw reads were filtered using Trimmomatic (v.0.39)[71] and clean reads were mapped to the Longmi4 genome using subjunc (v.2.0.1)[100]. Read counts and FPKM values were calculated using featureCounts (v.2.0.1)[101] and the differential expression of the genes between wild and domesticated accessions was analyzed using DESeq2 (v.1.32.0)[102]. Genes with an adjusted $P \leq 0.05$ and absolute(fold change) ≥ 1.5 were defined as the population's differentially expressed genes (pop-DEGs). Gene Ontology (GO) and Pfam annotation of pop-DEGs were performed with InterProScan (v.5.52-86.0)[92], while Kyoto Encyclopedia of Genes and Genomes (KEGG) annotation[103] was carried out with BlastKOALA (v.2.2)[104] and KofamKOALA[105]. Finally, the significantly enriched GO terms and KEGG categories were identified using a hypergeometric enrichment test in the R package clusterProfiler (v.4.2.2)[106], with a $P \leq 0.05$ as the threshold for significance.

SNP-based and PAV-based GWAS

We conducted an SNP-GWAS analysis on 43 phenotypes by using 1,890,542 SNPs with an MAF ≥ 0.05 and a missing rate ≤ 0.1. The missing SNP data were imputed with Beagle (v.4.1)[107]. Then, EMMAX (v.beta-07Mar2010)[108] was used for the association analysis incorporating a Balding–Nichols kinship matrix. The uniform threshold was set at 0.05/*n* (*n* represents the total number of SNPs) for the SNP-GWAS and the significance threshold was approximately $P = 10^{-8}$. In addition, we conducted a PAV-GWAS analysis using 19,492 PAVs with an MAF ≥ 0.05 and a missing rate ≤ 0.5. The PAV-GWAS threshold was set at 0.05/*n* (*n* represents the total number of PAVs); the significance threshold was approximately $P = 10^{-6}$. The associations were considered to be reliable only if they occurred at the same location for at least 2 years or in multiple locations.

Finally, we searched for significantly associated SNPs within 200 kb upstream and downstream regions to detect the potential regions of interest in the GWAS analysis. If significant SNPs were detected, we extended the search to the next 200-kb interval until no more significant SNPs were found. The boundaries of the candidate regions were defined based on the last significantly associated SNP in that region. To further identify the potential candidate genes within the candidate regions, we analyzed the Haps of the protein-coding genes using CandiHap (v.1.0.1) (https://github.com/guokai8/CandiHap). The genes with Haps significantly correlated with the phenotypes were considered as potential candidate genes.

Functional verification of *longmi038370*

To validate the function of *longmi038370*, we knocked out its orthologous gene *SiLG1* (*Seita.3G022100*) in foxtail millet using CRISPR–Cas9 genome editing. Single-guide RNAs (sgRNAs) were designed according to the sequence of foxtail millet *SiLG1*, using targetDesign (http://skl.scau.edu.cn/targetdesign/). The sgRNA target to the third exon of *SiLG1* was selected (Supplementary Fig. 33a) and the pYLCRISPRCas9-MH vector was used for genome-editing[109]. The primers used for vector construction were SiLG1-gR:AAGAAGCTGTGGATCCCAAGgttttagagctagaaat and SiLG1-OsU6a:CTTGGGATCCACAGCTTCTTcggcagccaagccagca. The CRISPR *Silg1* mutants were generated by editing *SiLG1* in foxtail millet (Ci846) through *Agrobacterium tumefaciens*-mediated transformation. Three independent CRISPR mutants were obtained and verified using Sanger sequencing. Ligule and panicle traits, such as BRM were measured in three mutations using five plants.

Geographical map generation

Information about the geographical location of the world sampled accessions in this study was generated using the ggmap package in R (v.4.1.0) and ArcGIS (v.10.2) (https://www.arcgis.com/). Monthly climate data for minimum, mean and maximum precipitation were retrieved from WorldClim[110].

Statistics

Statistical analyses and plotting were performed in R (v.4.1.0) using built-in functions and third-party R packages including tidyverse (v.1.3.1), ggplot2 (v.3.4.3), ggpubr (v.0.4.0) and agricolae (v.1.3-5). A two-tailed Wilcoxon rank-sum test was used to compare the difference of expression or phenotype between two groups with the R built-in function wilcox.test. A one-way analysis of variance was used to determine differences among groups. Pairwise comparisons were conducted using the least significant difference (LSD) method with Bonferroni correction for multiple comparisons using the function LSD.test in the third-party R package agricolae (v.1.3-5). Pearson correlation coefficients (*R*) and *P* values were calculated with the R function cor.test; fitted curves and 95% confidence intervals for linear regression were also calculated.

Reporting summary

Further information on research design is available in the Nature Portfolio Reporting Summary linked to this article.

Data availability

The raw sequences of 516 accessions (BioProject ID: PRJNA603255), the PacBio HiFi reads and RNA-seq data of 32 accessions (BioProject ID: PRJNA847741) and the Hi-C sequences of BC170 and BC418 (BC170: SRR17710547, SRR17710548, SRR17710549 and SRR17710550; BC418: SRR17710545, SRR17710546, SRR17710553 and SRR17710554) have been deposited with the Sequence Read Archive. The assembled pangenome sequences and gene and transposable element annotations are available at *Zenodo* (https://doi.org/10.5281/zenodo.6627574). The assembled pangenome sequences have also been deposited with the NCBI genome database; their accession numbers (JAVRMQ000000000–JAVRNV000000000) are listed in Supplementary Table 3. The phenotype data are available at *Zenodo* (https://doi.org/10.5281/zenodo.7749727). All study data are included in the main article and supplementary materials. All broomcorn millet accessions are available at the National Crop Genebank of China. Source data are provided with this paper.

Code availability

All codes and tools used in this study are described in the Methods. Codes are available at *Zenodo* (https://doi.org/10.5281/zenodo.8373683)[111].

References

70. Wang X. & Wang L. *Descriptors and Data Standard of Broomcorn Millet* (*Panicum miliaceum L.*) (China Agriculture Press, 2006).
71. Bolger, A. M., Lohse, M. & Usadel, B. Trimmomatic: a flexible trimmer for Illumina sequence data. *Bioinformatics* **30**, 2114–2120 (2014).
72. Li, H. & Durbin, R. Fast and accurate short read alignment with Burrows–Wheeler transform. *Bioinformatics* **25**, 1754–1760 (2009).
73. Chiang, C. et al. SpeedSeq: ultra-fast personal genome analysis and interpretation. *Nat. Methods* **12**, 966–968 (2015).
74. McKenna, A. et al. The Genome Analysis Toolkit: a MapReduce framework for analyzing next-generation DNA sequencing data. *Genome Res.* **20**, 1297–1303 (2010).
75. Durand, N. C. et al. Juicer provides a one-click system for analyzing loop-resolution Hi-C experiments. *Cell Syst.* **3**, 95–98 (2016).
76. Durand, N. C. et al. Juicebox provides a visualization system for Hi-C contact maps with unlimited zoom. *Cell Syst.* **3**, 99–101 (2016).
77. Wang, K., Li, M. & Hakonarson, H. ANNOVAR: functional annotation of genetic variants from high-throughput sequencing data. *Nucleic Acids Res.* **38**, e164 (2010).
78. Nguyen, L. T., Schmidt, H. A., von Haeseler, A. & Minh, B. Q. IQ-TREE: a fast and effective stochastic algorithm for estimating maximum-likelihood phylogenies. *Mol. Biol. Evol.* **32**, 268–274 (2015).
79. Purcell, S. et al. PLINK: a tool set for whole-genome association and population-based linkage analyses. *Am. J. Hum. Genet.* **81**, 559–575 (2007).
80. Zhang, C., Dong, S.-S., Xu, J.-Y., He, W.-M. & Yang, T.-L. PopLDdecay: a fast and effective tool for linkage disequilibrium decay analysis based on variant call format files. *Bioinformatics* **35**, 1786–1788 (2019).
81. Jombart, T. adegenet: a R package for the multivariate analysis of genetic markers. *Bioinformatics* **24**, 1403–1405 (2008).
82. Danecek, P. et al. The variant call format and VCFtools. *Bioinformatics* **27**, 2156–2158 (2011).
83. Quinlan, A. R. & Hall, I. M. BEDTools: a flexible suite of utilities for comparing genomic features. *Bioinformatics* **26**, 841–842 (2010).
84. Ou, S. & Jiang, N. LTR_retriever: a highly accurate and sensitive program for identification of long terminal repeat retrotransposons. *Plant Physiol.* **176**, 1410–1422 (2018).

85. Rhie, A., Walenz, B. P., Koren, S. & Phillippy, A. M. Merqury: reference-free quality, completeness, and phasing assessment for genome assemblies. *Genome Biol.* **21**, 245 (2020).
86. Li, H. Minimap2: pairwise alignment for nucleotide sequences. *Bioinformatics* **34**, 3094–3100 (2018).
87. Thorvaldsdóttir, H., Robinson, J. T. & Mesirov, J. P. Integrative Genomics Viewer (IGV): high-performance genomics data visualization and exploration. *Brief. Bioinform.* **14**, 178–192 (2013).
88. Stanke, M., Diekhans, M., Baertsch, R. & Haussler, D. Using native and syntenically mapped cDNA alignments to improve *de novo* gene finding. *Bioinformatics* **24**, 637–644 (2008).
89. Korf, I. Gene finding in novel genomes. *BMC Bioinformatics* **5**, 59 (2004).
90. Kim, D., Paggi, J. M., Park, C., Bennett, C. & Salzberg, S. L. Graph-based genome alignment and genotyping with HISAT2 and HISAT-genotype. *Nat. Biotechnol.* **37**, 907–915 (2019).
91. Kovaka, S. et al. Transcriptome assembly from long-read RNA-seq alignments with StringTie2. *Genome Biol.* **20**, 278 (2019).
92. Jones, P. et al. InterProScan 5: genome-scale protein function classification. *Bioinformatics* **30**, 1236–1240 (2014).
93. Flynn, J. M. et al. RepeatModeler2 for automated genomic discovery of transposable element families. *Proc. Natl Acad. Sci. USA* **117**, 9451–9457 (2020).
94. Li, W. & Godzik, A. Cd-hit: a fast program for clustering and comparing large sets of protein or nucleotide sequences. *Bioinformatics* **22**, 1658–1659 (2006).
95. Emms, D. M. & Kelly, S. OrthoFinder: phylogenetic orthology inference for comparative genomics. *Genome Biol.* **20**, 238 (2019).
96. Wang, D., Zhang, Y., Zhang, Z., Zhu, J. & Yu, J. KaKs_Calculator 2.0: a toolkit incorporating gamma-series methods and sliding window strategies. *Genomics Proteomics Bioinformatics* **8**, 77–80 (2010).
97. Zhang, Z. et al. ParaAT: a parallel tool for constructing multiple protein-coding DNA alignments. *Biochem. Biophys. Res. Commun.* **419**, 779–781 (2012).
98. Katoh, K., Misawa, K., Kuma, K. & Miyata, T. MAFFT: a novel method for rapid multiple sequence alignment based on fast Fourier transform. *Nucleic Acids Res.* **30**, 3059–3066 (2002).
99. Chen, S. et al. Paragraph: a graph-based structural variant genotyper for short-read sequence data. *Genome Biol.* **20**, 291 (2019).
100. Liao, Y., Smyth, G. K. & Shi, W. The Subread aligner: fast accurate and scalable read mapping by seed-and-vote. *Nucleic Acids Res.* **41**, e108 (2013).
101. Liao, Y., Smyth, G. K. & Shi, W. featureCounts: an efficient general purpose program for assigning sequence reads to genomic features. *Bioinformatics* **30**, 923–930 (2014).
102. Love, M. I., Huber, W. & Anders, S. Moderated estimation of fold change and dispersion for RNA-seq data with DESeq2. *Genome Biol.* **15**, 550 (2014).
103. Kanehisa, M. & Goto, S. KEGG: Kyoto Encyclopedia of Genomes. *Nucleic Acids Res.* **28**, 27–30 (2000).
104. Kanehisa, M., Sato, Y. & Morishima, K. BlastKOALA and GhostKOALA: KEGG tools for functional characterization of genome and metagenome sequences. *J. Mol. Biol.* **428**, 726–731 (2016).
105. Aramaki, T. et al. KofamKOALA: KEGG Ortholog assignment based on profile HMM and adaptive score threshold. *Bioinformatics* **36**, 2251–2252 (2020).
106. Yu, G., Wang, L.-G., Han, Y. & He, Q.-Y. clusterProfiler: an R package for comparing biological themes among gene clusters. *OMICS* **16**, 284–287 (2012).
107. Browning, B. L. & Browning, S. R. A unified approach to genotype imputation and haplotype-phase inference for large data sets of trios and unrelated individuals. *Am. J. Hum. Genet.* **84**, 210–223 (2009).
108. Kang, H. M. et al. Variance component model to account for sample structure in genome-wide association studies. *Nat. Genet.* **42**, 348–354 (2010).
109. Ma, X., Zhu, Q., Chen, Y. & Liu, Y.-G. CRISPR/Cas9 platforms for genome editing in plants: developments and applications. *Mol. Plant* **9**, 961–974 (2016).
110. Fick, S. E. & Hijmans, R. J. WorldClim 2: new 1-km spatial resolution climate surfaces for global land areas. *Int. J. Climatol.* **37**, 4302–4315 (2017).
111. Chen, J. Pan-genome analysis reveals genomic variations associated with domestication traits in broomcorn millet. *Zenodo* https://doi.org/10.5281/zenodo.8373683 (2023).

Acknowledgements

We thank M. Chen, F. Lu and N. Wang for their valuable comments and feedback on this manuscript. This work was funded by grants from the National Key R&D Program of China (grant no. 2019YFD1000700/2019YFD1000701 to S.T.; grant no. 2021YFF1000100/2021YFF1000103 to X.D.; and grant no. 2022YFD1400800/2022YFD1400803 to X.Z.), the China Agricultural Research System (grant no. CARS-06-13.5 to X.D.), the Agricultural Science and Technology Innovation Program of the Chinese Academy of Agricultural Sciences (G.J.), the Strategic Priority Research Program of the Chinese Academy of Sciences (grant no. XDPB16 to J. Chen), the National Natural Science Foundation of China (grant no. 32241038 to S.T. and grant no. U21A20216 to H.Z.) and the Open Research Fund Program of the State Key Laboratory of Integrated Management of Pest Insects and Rodents (grant no. IPM2108 to J. Cui).

Author contributions

X.D., S.T. and J. Chen. conceived and designed the study. M.L., P.L. and H.Z. prepared the materials and coordinated the field phenotyping. Y. Liu, Y. Liao and W.C. performed the genome assembly, annotation, and the pangenome and structural variation analyses. W.G., J. Chen., Q.H., Hongru Wang and Y.Z. performed the population genetics analysis. Y.W., W.G. and M.L. performed the GWAS analysis. K.D., R.R., T.Y., L.Z., M.Q., Z.L., M.Z., Haigang Wang, J.W., Z.Q., Haiquan Li, Y.J., G.L., X.S., Y. Deng, Hai Li, F.Y., Y. Dong, Q.L., T.L., W.Y., P.L. and H.Z. contributed to the field phenotyping. S.T., W.Z. and Y.G. generated and analyzed the molecular work on transgenic plants. J. Chen., Y. Liu, W.G., M.L., Y.W., Y. Liao, J. Cui, Hongru Wang, Y.Z., X.Z., G.J. and X.D. wrote and revised the paper.

Competing interests

The authors declare no competing interests.

Additional information

Supplementary information The online version contains supplementary material available at https://doi.org/10.1038/s41588-023-01571-z.

Correspondence and requests for materials should be addressed to Jinfeng Chen, Sha Tang or Xianmin Diao.

Peer review information *Nature Genetics* thanks Aureliano Bombarely and the other, anonymous, reviewer(s) for their contribution to the peer review of this work.

Reprints and permissions information is available at www.nature.com/reprints.

nature portfolio

Corresponding author(s): Jinfeng Chen, Sha Tang, and Xianmin Diao

Last updated by author(s): Oct 14, 2023

Reporting Summary

Nature Portfolio wishes to improve the reproducibility of the work that we publish. This form provides structure for consistency and transparency in reporting. For further information on Nature Portfolio policies, see our Editorial Policies and the Editorial Policy Checklist.

Statistics

For all statistical analyses, confirm that the following items are present in the figure legend, table legend, main text, or Methods section.

n/a | Confirmed

□ ☒ The exact sample size (*n*) for each experimental group/condition, given as a discrete number and unit of measurement

□ ☒ A statement on whether measurements were taken from distinct samples or whether the same sample was measured repeatedly

□ ☒ The statistical test(s) used AND whether they are one- or two-sided
Only common tests should be described solely by name; describe more complex techniques in the Methods section.

□ ☒ A description of all covariates tested

□ ☒ A description of any assumptions or corrections, such as tests of normality and adjustment for multiple comparisons

□ ☒ A full description of the statistical parameters including central tendency (e.g. means) or other basic estimates (e.g. regression coefficient) AND variation (e.g. standard deviation) or associated estimates of uncertainty (e.g. confidence intervals)

□ ☒ For null hypothesis testing, the test statistic (e.g. *F*, *t*, *r*) with confidence intervals, effect sizes, degrees of freedom and *P* value noted
Give P values as exact values whenever suitable.

☒ □ For Bayesian analysis, information on the choice of priors and Markov chain Monte Carlo settings

☒ □ For hierarchical and complex designs, identification of the appropriate level for tests and full reporting of outcomes

□ ☒ Estimates of effect sizes (e.g. Cohen's *d*, Pearson's *r*), indicating how they were calculated

Our web collection on statistics for biologists contains articles on many of the points above.

Software and code

Policy information about availability of computer code

Data collection

1, Seed dimensions including seed width, seed length, and seed weight were measured with SC-G software (Hangzhou Wanshen Detection Technology)
2, High-fidelity (HiFi) long reads were collected using the Circular Consensus Sequencing (CCS) analysis application with SMRT Link.

Data analysis

1, The raw reads were filtered by removing low-quality bases and sequencing adaptors with Trimmomatic (v0.39)
2, Clean reads were aligned to the Longmi4 genome with BWA-MEM using speedseq (v0.0.2)
3, Genomic variations including SNPs and INDELs were performed with GATK UnifiedGenotyper (v3.8)
4, Fourfold degenerate synonymous sites (4DTv) were obtained from ANNOVAR (v2020-06-08)
5, 4DTv sites were used to construct a maximum likelihood phylogenetic tree using IQ-TREE (v2.1.4-beta)
6, Principle component analysis (PCA) of 516 broomcorn millet accessions was conducted by plink (v1.90b6.18)
7, Population structure analysis was performed by ADMIXTURE (v1.3.0), fastSTRUCTURE (v1.0), STRUCTURE (v2.3.4), DAPC in adegenet (v2.1.8)
8, Linkage disequilibrium was calculated with PopLDDecay (v3.41)
9, Artificial selection sweeps during domestication and improvement were detected by combining cross-population composite likelihood ratio test (XP-CLR v1.0)
10, Top 5% was used as a threshold for significance. XP-CLR scores were then smoothed using 100-kb windows with 10-kb steps on each chromosome. VCFtools (v0.1.13)
11, Overlap among selection sweeps detected by XP-CLR, πwild / πcultivar, Fst were identified with BEDTools (v2.29.1)
12, Raw contigs were generated from HiFi long reads using Hifiasm (v0.14.2-r315)
13, Contigs were anchored onto chromosomes using RagTag (v2.0.1)
14, To evaluate the quality of assembly, we first performed gene completeness analysis with BUSCO (v4.0.6) and repeat completeness analysis

with the LTR assembly index (LAI) using LTR_retriever (v2.9.0)
15, Hi-C reads were manually inspected with Juicebox (v1.11.08)
16, Gene annotation was performed on each assembly using the MAKER2 pipeline (v2.31.11)
17, Repetitive sequences in each de novo assembly were annotated with RepeatModeler (v2.0.1)
18, The non-redundant protein sequences were clustered into gene families using OrthoFinder (v2.5.4)
19, The ratios of Non-synonymous/Synonymous mutation (Ka/Ks) for each gene of the pan-genome were calculated using KaKs_Calculator (v2.0)
20, A reference-based alignment approach named PopASSYsv (https://github.com/yiliao1022/PoPASSYSV) was used to call and genotype structural variations from our population-scale and highly contiguous genome assemblies.
21, Merged deletions and insertions were genotyped across 516 accessions by short-read data using paragraph (v2.3)
22, Gene Ontology (GO) and Pfam annotation of Pop-DEGs were performed with InterProScan (v5.52-86.0)
23, Kyoto Encyclopedia of Genes and Genomes (KEGG) annotation was performed with BlastKOALA (v2.2) and KofamKOALA
24, RNA seq reads were mapped to the Longmi4 genome using subjunc (v2.0.1)
25, Read counts and FPKM values were calculated using featureCounts (v2.0.1)
26, The differential expression of the genes was analyzed using DESeq2 (v1.32.0)
27, Enriched GO terms and KEGG categories were identified with R package ClusterProfiler (v4.2.2)
28, The missing SNP data were imputed with Beagle (v4.1)
29, The association analysis was performed with EMMAX (vbeta-07Mar2010)
30, The haplotypes of protein-coding genes within candidate regions were analyzed with CandiHap (v1.0.1)
31, The geographical location information of the world sampled accessions in this study are generated using ggmap package in R (v4.1.0) and ArcGIS (v10.2, https://www.arcgis.com/) software
32, Statistical analyses and plotting were performed in R (v.4.1.0) using built-in functions and third-part R packages including tidyverse (v1.3.1), ggplot2 (v.3.4.3), ggpubr (v.0.4.0) and agricolae (v1.3-5)
33, Two-tailed Wilcoxon's rank-sum test was used to compare the difference of expression or phenotype between two groups with R built-in functions wilcox.test
34, One-way ANOVA test was used to determine differences among groups. Pairwise comparison was conducted by the least significant difference (LSD) method with Bonferroni correction for multiple comparisons using function LSD.test in third-part R package agricolae (v1.3-5)
35, Pearson's correlation coefficient (R) and P value was calculated with R function cor.test, fitted curves and 95% confidence intervals for linear regression were also calculated

Code availability
All codes or tools used in this study are described in the methods. Codes are available at Zenodo (https://doi.org/10.5281/zenodo.8373683).

For manuscripts utilizing custom algorithms or software that are central to the research but not yet described in published literature, software must be made available to editors and reviewers. We strongly encourage code deposition in a community repository (e.g. GitHub). See the Nature Portfolio guidelines for submitting code & software for further information.

Data

Policy information about availability of data

All manuscripts must include a data availability statement. This statement should provide the following information, where applicable:

- Accession codes, unique identifiers, or web links for publicly available datasets
- A description of any restrictions on data availability
- For clinical datasets or third party data, please ensure that the statement adheres to our policy

The raw sequences of 516 accessions (BioProject accession no. PRJNA603255), PacBio HiFi reads and RNA-Seq data of 32 accessions (BioProject accession no. PRJNA847741), and the Hi-C sequences of BC170 and BC418 (BC170: SRR17710547-50; BC418: SRR17710545-6, SRR17710553-4) have been deposited in the National Center for Biotechnology Information SRA. The assembled pan-genome sequences and gene and transposable element annotations are available at Zenodo (https://doi.org/10.5281/zenodo.6627574). The assembled pan-genome sequences have also been deposited into the NCBI genome database and their accession numbers (JAVRMQ000000000- JAVRNV000000000) were listed in Supplementary Table 3. The phenotype data are available at Zenodo (https://doi.org/10.5281/zenodo.7749727). All study data are included in the main article and Supplementary Materials. All broomcorn millet accessions are available at the National Crop Genebank of China.

Human research participants

Policy information about studies involving human research participants and Sex and Gender in Research.

Reporting on sex and gender	N/A
Population characteristics	N/A
Recruitment	N/A
Ethics oversight	N/A

Note that full information on the approval of the study protocol must also be provided in the manuscript.

Field-specific reporting

Please select the one below that is the best fit for your research. If you are not sure, read the appropriate sections before making your selection.

☒ Life sciences ☐ Behavioural & social sciences ☐ Ecological, evolutionary & environmental sciences

For a reference copy of the document with all sections, see nature.com/documents/nr-reporting-summary-flat.pdf

Life sciences study design

All studies must disclose on these points even when the disclosure is negative.

Sample size	The sample size of resequencing samples (516) were chosen based on accessions available at the National Crop Genebank of China to cover geographic distribution of broomcorn millet. The sample size (32) of pan-genome samples were chosen based on previous pan-genome studies (1-3) to represent population diversity of broomcorn millet. Reference: 1, Liu, Y. et al. Pan-genome of wild and cultivated soybeans. Cell 182, 162-176 (2020). 2, Hufford, M. B. et al. De novo assembly, annotation, and comparative analysis of 26 diverse maize genomes. Science 373, 655-662 (2021). 3, Qin, P. et al. Pan-genome analysis of 33 genetically diverse rice accessions reveals hidden genomic variations. Cell 184, 3542-3558 (2021).
Data exclusions	We did not exclude any data from data analyses.
Replication	RNAseq experiments were performed with three biological replicates. Trait evaluation of 516 accessions were performed with three biological replicates per accession at seven sites. Trait evaluation of CRISPR mutants were performed with five biological replicates. All replications were successful and reported in the manuscript.
Randomization	For trait evaluation, we randomly sampled three plants out of 80 plants per accession in the field. For RNA and DNA extractions, we randomly sampled 3 plants out of 10-15 plants in the greenhouse or growth chamber.
Blinding	Blinding is not necessary for sampling accessions for genome sequencing. The samples for genome sequencing of broomcorn millets were selected based on their geographic distribution, phylogenetic tree as we need to cover the geographic distribution and genetic diversity of this species. The investigators were blinded to population structure or origin of accessions when collecting traits in the field.

Reporting for specific materials, systems and methods

We require information from authors about some types of materials, experimental systems and methods used in many studies. Here, indicate whether each material, system or method listed is relevant to your study. If you are not sure if a list item applies to your research, read the appropriate section before selecting a response.

Materials & experimental systems

n/a	Involved in the study
☒	☐ Antibodies
☒	☐ Eukaryotic cell lines
☒	☐ Palaeontology and archaeology
☒	☐ Animals and other organisms
☒	☐ Clinical data
☒	☐ Dual use research of concern

Methods

n/a	Involved in the study
☒	☐ ChIP-seq
☒	☐ Flow cytometry
☒	☐ MRI-based neuroimaging